Effective field theory of thermal Casimir interactions between anisotropic particles

Robert C. Haussman* and Markus Deserno†

Department of Physics, Carnegie Mellon University, 5000 Forbes Avenue, Pittsburgh, Pennsylvania 15213, USA

(Received 22 December 2013; published 3 June 2014)

We employ an effective field theory (EFT) approach to study thermal Casimir interactions between objects bound to a fluctuating fluid surface or interface dominated by surface tension, with a focus on the effects of particle anisotropy. The EFT prescription disentangles the constraints imposed by the particles' boundaries from the calculation of the interaction free energy by constructing an equivalent point particle description. The finite-size information is captured in a derivative expansion that encodes the particles' response to external fields. The coefficients of the expansion terms correspond to generalized tensorial polarizabilities and are found by matching the results of a linear response boundary value problem computed in both the full and effective theories. We demonstrate the versatility of the EFT approach by constructing the general effective Hamiltonian for a collection of particles of arbitrary shapes. Taking advantage of the conformal symmetry of the Hamiltonian, we discuss a straightforward conformal mapping procedure to systematically determine the polarizabilities and derive a complete description for elliptical particles. We compute the pairwise interaction energies to several orders for nonidentical ellipses as well as their leading-order triplet interactions and discuss the resulting preferred pair and multibody configurations. Furthermore, we elaborate on the complications that arise with pinned particle boundary conditions and show that the powerlike corrections expected from dimensional analysis are exponentially suppressed by the leading-order interaction energies.

DOI: 10.1103/PhysRevE.89.062102 PACS number(s): 05.40.−a, 03.50.−z, 68.03.Kn

I. INTRODUCTION

When constraints such as extended or compact boundaries are imposed on a fluctuating field, this alters the underlying energy spectrum. If these boundary constraints are due to physical objects, field-mediated interactions are generally induced between them. A typical example, first discussed by Casimir in 1948, is a pair of neutral, conducting plates placed in a vacuum. Such plates experience attractive forces because their boundaries constrain the vacuum fluctuations of the electromagnetic field [1,2]. Casimir-type interactions, however, naturally arise in a variety of classical systems as well. In particular, particles or other localized inhomogeneities bound to a soft surface will constrain the surface locally and modify its thermal fluctuation spectrum, leading to surface-mediated interactions [3–14]. In this article, we will consider a collection of anisotropic particles bound to a fluid surface, whose energetics is dominated by surface tension.

The study of fluctuation-induced interactions between compact objects is complicated by the fact that the boundaries break translational symmetry, rendering the partition function more difficult than that of the free field. Even if the latter is trivial (say, because the action is quadratic in the field), the constraints imposed by the objects, which themselves might be subject to rigid body motions or even more complicated modes of deformation, need to be enforced—either in the functional integrals or by suitably scale separating the problem. For the case of axisymmetric objects (such as spheres or circular disks) on surface-tension dominated fluid surfaces, this problem has been investigated in a number of studies, either by constraining the partition function [5–7,9,11,15,16] or by scale separating the problem using the tools of effective field theory (EFT) [12,13]. In the asymptotic regime of large distances one finds power-law interactions in the separation r, unless the objects are pinned (stationary), in which case the interactions become very long ranged, proportional to $\log\log r$. Of course, at closer distances higher-order terms add corrections to the asymptotic power law, which become substantial as the separation between particles become comparable to their size, since in fact the interaction is known to diverge upon surface contact [6,13,17].

Relaxing axisymmetry leads to a number of interesting anisotropic effects, but the interaction exhibits the same leading-order r-dependence as the symmetric case, as found by Oettel and coworkers [7,8] by explicitly studying ellipses. However, at higher orders in the pinned case, their analysis [8] found additional terms $\sim (r^{2n}\log[4r/(a+b)])^{-1}$, where a and b are the principle axes of the ellipse. This is remarkable, because such terms do not vanish in the symmetric (circular) limit $a \to b$, whereas a regularized diagrammatic approach shows that every Feynman diagram involving both pinned ("monopole") and nonpinned ("higher-order multipole") boundary constraints vanishes in the relevant limit of a free surface. Here we trace back the origin of this discrepancy to a subtle noncommutation problem for two limits: Since the pinned constraints in a perturbative expansion do not affect the order of a diagram, they must be resummed, and the regularization of this infinite sum can only be removed *afterward*. This leads to the logarithmic corrections found by Noruzifar *et al.* [8], but derived in a very different manner.

As we have mentioned, calculating surface-mediated interactions between objects is surprisingly nontrivial, with the major difficulty arising from the constraints imposed on the partition sum. Previously, these constraints were managed by including appropriate delta functions in the integration

*roberthaussman@cmu.edu
†deserno@andrew.cmu.edu

measure, which in turn was handled by introducing a set of auxiliary fields (see, for instance, Ref. [11]). A more general version of this approach has been developed in an electromagnetic context by Emig *et al.* [18,19], in which the particle constraints enter into the effective energy through scattering matrix coefficients. This method has also recently been appropriated for particles at a fluid interface by Noruzifar *et al.* [15,16]. In the case of two-dimensional critical systems, conformal field theory (CFT) techniques have been developed to treat special cases [17,20,21], and further generalized for pairs of arbitrarily shaped objects by Bimonte *et al.* [22]. Although the CFT technique is powerful, and in certain cases leads to exact solutions, it is limited to systems with conformal symmetry.

To get an alternative handle on the abovementioned difficulties, we will instead employ an effective field theory (EFT) approach and generalize the methods introduced in Refs. [12,13]. Typically, one is interested in the physics at a certain scale of a potentially multiscale problem. In our case, we are interested in the long distance physics. The EFT approach makes this scale manifest by effectively integrating out the short distance physics and systematically encoding the small scale information (finite size of particles, boundary conditions, etc.) as numerical couplings in the Hamiltonian. In doing so, we are reverting to a controlled point-particle description that allows for calculations of interaction energies to high orders (or in the case of Ref. [13], to *all* orders) without any conceptual difficulties.

In this paper, we will investigate the effects of anisotropies by objects with arbitrary geometries, with particular emphasis on the case of elliptic boundaries to make connection with previous studies. To our knowledge this is the first application of EFT to thermally fluctuating systems that explores the full tensorial nature of Wilson coefficients on the worldline, and thus serves as a good illustration for how the power of EFT is not restricted to highly symmetric situations. In the next section, we will discuss the surface energetics and boundary conditions imposed by the particles, as well as elaborate on the EFT formalism. In Sec. III we will construct the effective Hamiltonian for particles of arbitrary shape and then discuss the simplification for ellipses. We then discuss a matching procedure that takes advantage of conformal mapping, valid for arbitrarily shaped particles, and then compute the full set of Wilson coefficients (polarizabilities) for ellipses of arbitrary aspect ratio. Since the case of pinned particles exhibits short-distance divergences, we introduce an appropriate regularization procedure and provide a detailed discussion of the matching for monopolelike terms. Finally, we comment on the limiting cases of rods and disks. In Sec. IV we discuss pair and multibody interactions. We begin with a pedagogical discussion of the diagrammatic rules for computing the interaction energies. Next, we calculate the pair interactions to several orders for various nonpinned boundary conditions and discuss preferred orientations. Furthermore, we calculate the leading-order multibody interactions and discuss the preferred three-body particle configurations and orientations. Since the monopole interactions require extra care, we relegate their discussion to Sec. V and provide a detailed account of the resummation of interaction terms. We then provide higher-order corrections to the pair and three-body interactions for pinned particles. Finally, we summarize and conclude in Sec. VI.

We note before proceeding that the reader may find the following pages rather dense with lengthy mathematical expressions. This is not due to complications in the EFT approach, but rather a result of demonstrating how far the analysis can be extended. In particular, we provide a detailed calculation of the full theory boundary value problem from a conformal mapping trick to determine the complete set of polarizabilities. However, the EFT approach disentangles this calculation from the rest of the description, and solving the boundary value problem for a complicated particle shape is generally difficult, but it is independent of EFT. In fact, this calculation may be done in any manner most convenient—even numerically—and the EFT approach will proceed in the same systematic fashion. Furthermore, we provide a fairly detailed discussion of the diagrammatic rules in hopes that this work may be approachable to a wide audience, regardless of their exposure to standard field theory techniques.

II. ENERGETICS AND FORMALISM

A. Surface energetics

The energetics of fluid-fluid interfaces is well described by the coarse grained Hamiltonian $\mathcal{H} = \sigma \int dA$, where σ is the surface tension (excess free energy per area). Since we will be interested in deviations about a flat ground-state surface, it is convenient to work in the *Monge gauge* [23] in which $h(\boldsymbol{x})$ is the orthogonal displacement from a base plane parametrized by $\boldsymbol{x} = (x, y)$ (see Fig. 1). In this representation the energy functional over the surface becomes

$$\mathcal{H}[h] = \sigma \int_{\mathcal{S}_{\rm pr}} d^2x \, \sqrt{g} = \sigma \int_{\mathcal{S}_{\rm pr}} d^2x \, \sqrt{1 + \left(\boldsymbol{\nabla} h(\boldsymbol{x})\right)^2}, \quad (1)$$

where $\mathcal{S}_{\rm pr}$ is projection of the surface onto the base plane and g is the metric determinant. In the *linearized Monge gauge*, applicable for small deformations in which $|\boldsymbol{\nabla} h| \ll 1$, we can perform a gradient expansion and keep the leading term. Up

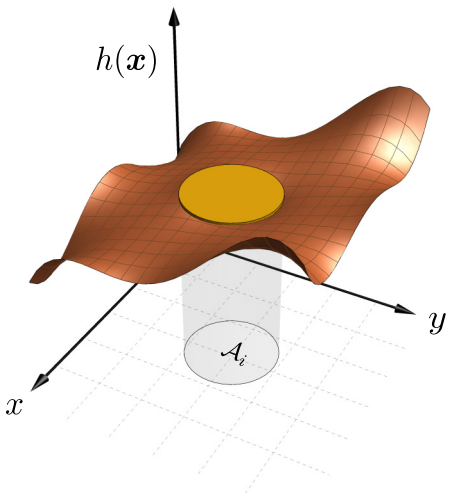

FIG. 1. (Color online) Illustration of the height function $h(\boldsymbol{x})$ in the Monge gauge. A flat particle is bound to a fluctuating surface and projects an area $\mathcal{A}$ onto the base plane.

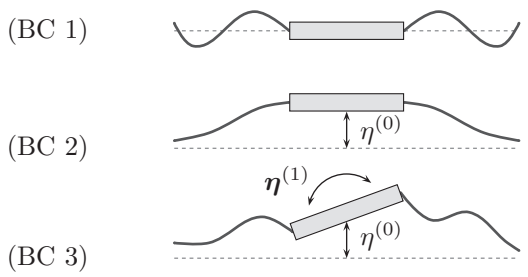

FIG. 2. Visual representation of the three boundary conditions. The freedom of the particle to fluctuate in height and tilt is parametrized by $\eta^{(0)}$ and $\boldsymbol{\eta}^{(1)}$, respectively.

to an irrelevant constant, the Hamiltonian becomes

$$\mathcal{H}[h] = \sigma \int_{\mathcal{S}_{\rm pr}} d^2x \, \frac{1}{2}(\nabla h)^2 + \text{const.} \tag{2}$$

With the inclusion of particles, the surface domain is given generally by $\mathcal{S}_{\rm pr} = \mathbb{R}^2 \setminus \bigcup_i \mathcal{A}_i$ where $\mathcal{A}_i$ is the area of the ith particle projected onto the base plane. The height function will assume a contact profile $h(\boldsymbol{x})|_{\partial\mathcal{A}_i} = h_i^{\rm ct}(\boldsymbol{x})|_{\partial\mathcal{A}_i}$ at each particle boundary $\partial\mathcal{A}_i$. In this paper we will consider flat particles, for which the contact profile may be written as $h_i^{\rm ct}(\boldsymbol{x}) = \eta_i^{(0)} + \boldsymbol{\eta}_i^{(1)} \cdot \boldsymbol{x}$, where $\eta^{(0)}$ and $\boldsymbol{\eta}^{(1)}$ parametrize the vertical position and tilt of the particle. Following the categorization of Ref. [6], we will consider three types of boundary conditions for each particle (see Fig. 2):

(BC 1) The position and orientation is fixed: $h|_{\partial\mathcal{A}_i} = 0$.

(BC 2) The vertical position is allowed to fluctuate: $h|_{\partial\mathcal{A}_i} = \eta_i^{(0)}$.

(BC 3) The vertical position and tilt are both allowed to fluctuate: $h|_{\partial\mathcal{A}_i} = (\eta_i^{(0)} + \boldsymbol{\eta}_i^{(1)} \cdot \boldsymbol{x})|_{\partial\mathcal{A}_i}$.

In the above categories, $\eta^{(0)}$ and $\boldsymbol{\eta}^{(1)}$ take on the role of *free* parameters and reflect the zero mode(s) of the boundary conditions. That is, these parameters may fluctuate freely without costing any energy. The implications of these boundary conditions will be explored further when we construct the effective theory.

B. Fluctuation-induced interactions

The particle boundaries locally constrain the thermal fluctuations which thereby induce surface-mediated interactions, even for flat particles. The interaction potentials will appear as differences associated free energy $\mathcal{F}$, and will depend on the spatial arrangements and orientations of the particles. The free energy is related to the partition function Z, and is given formally by the functional integral,

$$e^{-\beta\mathcal{F}} = Z \equiv \int \mathcal{D}'h \, e^{-\beta\mathcal{H}[h]}, \tag{3}$$

where $\beta = 1/k_{\rm B}T$. The prime on the measure reminds us that we integrate only over the field configurations that obey the constraints at the particle boundaries. As mentioned previously, the computational difficulties lie in enforcing this constraint.

Since we are interested in the long-distance physics, we will instead reformulate the problem by treating the particles as points in such a way that the short-distance physics is still retained. This entails including a series of additional terms in the Hamiltonian; however, these terms can be handled perturbatively, for which standard field theory techniques are applicable.

C. The EFT approach

The key to the EFT approach is that at large distances, the effects of an embedded particle will appear as coming from a localized source. That is, the short-distance particle characteristics will manifest themselves as local terms in the Hamiltonian. As the interactions should diminish at large distances, these local terms should scale as powers of s/r, where s is a length scale representing the object size and r is the distance from the particle. Accordingly, we construct the effective Hamiltonian as $\mathcal{H}_{\rm eff} = \mathcal{H}_0 + \Delta\mathcal{H}$, where the *bulk Hamiltonian* $\mathcal{H}_0$ describes the free surface [Eq. (1) with $\mathcal{S}_{\rm pr} = \mathbb{R}^2$] and the *worldline Hamiltonian* $\Delta\mathcal{H}$ contains the local terms resulting from boundary conditions of the particles. The partition function then becomes the unconstrained functional integral,

$$Z = \int \mathcal{D}h \, e^{-\beta\mathcal{H}_{\rm eff}} = \int \mathcal{D}h \, e^{-\beta\mathcal{H}_0} e^{-\beta\Delta\mathcal{H}}. \tag{4}$$

It will prove useful to cast the exponential of Eq. (4) in terms of the dimensionless field $\phi = h/\lambda$, where we have introduced the *molecular* length scale $\lambda = 1/\sqrt{\beta\sigma}$.[1] In particular, the gradient expansion of the bulk term becomes

$$\begin{aligned}\beta\mathcal{H}_0[\phi] &= \frac{1}{\lambda^2}\int_{\mathbb{R}^2} d^2x \, \sqrt{1+\lambda^2(\nabla\phi)^2} \\ &= \frac{1}{\lambda^2}\int_{\mathbb{R}^2} d^2x \, \left\{1 + \frac{\lambda^2}{2}(\nabla\phi)^2 - \frac{\lambda^4}{8}[(\nabla\phi)^2]^2 + \cdots\right\} \\ &= \int_{\mathbb{R}^2} d^2x \, \frac{1}{2}(\nabla\phi)^2 + \text{const} + O(\lambda^2).\end{aligned} \tag{5}$$

The overall constant is irrelevant and λ is very small so we are justified in dropping the remaining nonlinear $O(\lambda^2)$ terms.

In general, to construct $\Delta\mathcal{H}$ we must write down all possible local terms $C^{(k)}\mathcal{O}_k(\phi)$, or *operators* in the EFT language, that obey the symmetries of the particles. The prefactors $C^{(k)}$, called *Wilson coefficients*, encode the short distance particle information and will be determined later by a matching procedure. The sum of operators can be organized to form a power series in each of the physical scales, which will allow us to truncate the series to the desired order of accuracy in a consistent and controlled way. This series then appears as a derivative expansion, evaluated at the position of each particle. In our case, we note that there are two length scales: the characteristic particle size s, and the molecular scale λ. Since ϕ is dimensionless, the dimensions of each operator $\mathcal{O}_k(\phi)$ are carried by the derivatives. The length scale λ is associated with powers of ϕ, so to ensure $\beta\Delta\mathcal{H}$ is dimensionless, we find that the number of derivatives is associated with the powers of the particle size s. Hence, denoting the overall power of ϕ

[1] For water at room temperature, the surface tension is about 73 mN/m and hence the length scale $\lambda \approx 2$ Å, which is indeed comparable to the size of a water molecule.

by n_k and the total number of derivatives by d_k, we can write $\beta\Delta\mathcal{H}$ up to some unknown dimensionless (possibly tensor) coefficients $c^{(k)}$,

$$\beta\Delta\mathcal{H}[\phi] = \sum_\alpha \sum_k C_\alpha^{(k)} \mathcal{O}_k(\phi(\boldsymbol{x}_\alpha)) = \sum_\alpha \sum_k c_\alpha^{(k)} s_\alpha^{d_k} \lambda^{n_k-2} \mathcal{O}_k(\phi(\boldsymbol{x}_\alpha)), \tag{6}$$

where for each particle α, the operator is evaluated at its position $\boldsymbol{x}_\alpha$. This series, although complete, may include some redundancy. In particular, terms proportional to the Euler-Langrange equation of the bulk term are deemed redundant, as they can be removed by appropriate field redefinitions without affecting the physics [24]. We will later exploit this to simplify the construction of the particle EFT.

To determine the Wilson coefficients $C^{(k)}$, we must perform a matching procedure such that the EFT correctly reproduces the physics at large distances. That is, any observable calculated in the EFT must asymptotically match the result obtained by the *full theory* in Eq. (3). The aim then is to find a convenient observable such that its calculation in the full theory is as simple as possible. Given that we are interested in fluctuations, we employ the background field method in which we decompose the field via $\phi = \phi_{\rm bg} + \delta\phi$, where $\phi_{\rm bg}$ is an imposed (fixed) background field and $\delta\phi$ is the response, and match the response calculated in the full and effective theories.

III. EFT OF ELLIPSOIDAL PARTICLES

A. Effective Hamiltonian

We begin by noting that minimizing the surface Hamiltonian in the small gradient approximation gives the two-dimensional Laplace equation $\nabla^2\phi = 0$, whose solutions can always be broken up into a sum of holomorphic and antiholomorphic functions. This provides motivation to work directly in complex variables $\boldsymbol{z} = (z,\bar{z})$ with $z = x + iy$ and $\bar{z} = z^* = x - iy$. The metric then becomes

$$g_{\alpha\beta} \doteq \frac{1}{2}\begin{pmatrix} 0 & 1 \\ 1 & 0 \end{pmatrix}, \quad g^{\alpha\beta} \doteq 2\begin{pmatrix} 1 & 0 \\ 0 & 1 \end{pmatrix}. \tag{7}$$

The derivatives are given by $\partial \equiv \partial_z = (\partial_x - i\partial_y)/2$ and $\bar{\partial} \equiv \partial_{\bar{z}} = (\partial_x + i\partial_y)/2$, and Laplace's equation takes the form $4\partial\bar{\partial}\phi = 0$. The benefit of this coordinate transformation is that mixed derivatives on the field will always vanish. That is, in our derivative expansion we need only consider exclusively ∂ or $\bar{\partial}$ derivatives on each instance of the field.[2]

To construct the general EFT for anisotropic particles, we must be explicit about the symmetries and boundary conditions. Implied in the surface Hamiltonian is an up-down symmetry $\phi \to -\phi$; this carries over for particles with flat contact lines, limiting $\mathcal{O}_k(\phi)$ to even powers of ϕ.[3] Additionally, since $O(\lambda^2)$ terms are neglected in the linear Monge gauge, $\beta\Delta\mathcal{H}$ can be at most quadratic in the field ϕ. Hence, $\beta\Delta\mathcal{H}$ must be a derivative expansion *strictly* quadratic in ϕ. As mentioned previously, we are also free to remove terms containing the bulk Euler-Lagrange equations (i.e., terms containing $\partial\bar{\partial}\phi$), so instances of the field will never appear with mixed ∂, $\bar{\partial}$ derivatives. Together these conditions imply the worldline Hamiltonian for a single particle sitting at origin must take the form,

$$\beta\Delta\mathcal{H}[\phi] = \sum_{n,m\geqslant 0} \Big[C_{nm}\partial^n\phi\bar{\partial}^m\phi + \frac{1}{2}\chi_{nm}\partial^n\phi\partial^m\phi + \frac{1}{2}\bar{\chi}_{nm}\bar{\partial}^n\phi\bar{\partial}^m\phi \Big]_{z=\mathbf{0}}, \tag{8}$$

where the Wilson coefficients scale as powers of the characteristic particle size: $[C_{nm}] \sim [\chi_{nm}] \sim [\bar{\chi}_{nm}] \sim s^{n+m}$. Since $\beta\Delta\mathcal{H}$ must be real, $C_{mn} = (C_{nm})^*$ and $\bar{\chi} = \chi^*$. Furthermore, from the symmetry of derivatives it follows that χ and $\bar{\chi}$ are both symmetric tensors.

Equation (8) is the general form for *any* anisotropic particle. However, additional symmetries associated with the particle boundary conditions may lead to the vanishing of some terms. For example, in the case of circular disks considered in Refs. [12] and [13], there is a complete rotational symmetry $z \to e^{i\varphi}z$ for any angle φ, implying $C_{nm} \to C_{nm}\delta_{nm}$ and $\chi_{nm} = \bar{\chi}_{nm} = 0$. Hence anisotropies are encoded in the off-diagonal terms of C_{nm} as well as the χ and $\bar{\chi}$ tensors. For an ellipse, the symmetry is limited to discrete rotations by an angle π ($z \to -z$). Since the worldline Hamiltonian must obey this same symmetry, we find that Wilson coefficients for an ellipse are reduced to only those whose indices obey $n + m \in 2\mathbb{N}_0$.

The particle boundary conditions also put constraints on the Wilson coefficients. For (BC 1), Eq. (8) is the complete EFT, including the $n = m = 0$ terms. The vertical fluctuation freedom of (BC 2) implies a $\phi \to \phi + \text{const}$ translation symmetry at the particle boundary, which therefore forbids any $n = m = 0$ terms. The additional tilt freedom of (BC 3) implies that the Hamiltonian should be invariant under a shift of the field linear in z. This amounts to forbidding single derivatives on the field. That is, (BC 3) will additionally forbid any terms with $n = 1$ or $m = 1$.

B. Matching

As mentioned previously, to fix the Wilson coefficients we impose a background field and compare the corresponding response from the full and effective theories for a single particle. We first examine the EFT response for a general background. The form of the response will motivate a convenient choice of background field, which we will then apply to the full theory boundary value problem. We will perform the calculations first

[2]Strictly speaking, z and z^* are not independent. However, the formal manipulations can be justified by promoting x and y to complex numbers so that $(z,\bar{z}) \in \mathbb{C}^2$. The ∂ and $\bar{\partial}$ derivatives then follow the standard rules. After performing computations we can restrict the results to the "real surface" $\{(z,\bar{z}) \in \mathbb{C}^2 : \bar{z} = z^*\}$.

[3]A permanently deformed contact profile can be enforced by adding a source term linear in ϕ and localized to the particle position. For more details, see Ref. [13].

for (BC 2), and later discuss the modifications to accommodate (BC 1) and (BC 3).

1. *Effective response*

For a quadratic theory, the background field method amounts to a linear response problem. Setting $\phi = \phi_{\rm bg} + \delta\phi$ in Eq. (8) and taking the terms linear in $\delta\phi$ gives the effective source for this background. Without loss of generality, we will take the particle to be positioned at the origin as in Eq. (8) and the effective source becomes

$$\begin{aligned} J(z) &= -\left.\frac{\delta(\beta\Delta\mathcal{H})}{\delta\phi(z)}\right|_{\phi=\phi_{\rm bg}} \\ &= \sum_{n,m}(-1)^n\left\{C_{nm}\partial^n[\delta(z)\bar\partial^m\phi_{\rm bg}]\right. \\ &\quad \left. + \chi_{nm}\partial^n[\delta(z)\partial^m\phi_{\rm bg}]\right\} + \text{c.c.}, \end{aligned} \tag{9}$$

where c.c. stands for complex conjugate. The response is given by the convolution,

$$\delta\phi_{\rm EFT}(z) = \int d^2\zeta\, G(z-\zeta)J(\zeta), \tag{10}$$

where

$$G(z-\zeta) = -\frac{1}{4\pi}\log[(z-\zeta)(\bar z-\bar\zeta)] \tag{11}$$

is the Green function of the bulk Euler-Lagrange equation $-4\partial\bar\partial\phi = 0$, and $d^2\zeta = d(\mathrm{Re}\,\zeta)d(\mathrm{Im}\,\zeta)$. The final result is

$$\begin{aligned} \delta\phi_{\rm EFT}(z) &= -\sum_{n,m}(-1)^n\partial^n G(z) \\ &\quad \times [C_{nm}\bar\partial^m\phi_{\rm bg}(0) + \chi_{nm}\partial^m\phi_{\rm bg}(0)] + \text{c.c.} \end{aligned} \tag{12}$$

The form of both the effective source (9) and response (12) suggests choosing a general set of background multipole fields (rotated by an arbitrary angle φ),

$$\phi^{(n)}_{\rm bg}(\zeta;\varphi) = A^{(n)}(\zeta^n e^{-in\varphi} + \bar\zeta^n e^{in\varphi}), \tag{13}$$

since

$$\partial^m\phi^{(n)}_{\rm bg}(0) = A^{(n)}n!e^{-in\varphi}\delta_{nm} \tag{14}$$

is nonzero only for $n = m$. This immediately implies an interpretation analogous to two-dimensional electrostatics: The background field polarizes the object, leading to an induced source of boundary "charges" which generate the response field (12). With this analogy in mind, we will refer to the Wilson coefficients as *polarizabilities*. Plugging the multipole background into Eq. (12) and using

$$\partial^n G(z) = \frac{(-1)^n}{4\pi}\frac{(n-1)!}{z^n} \tag{15}$$

gives the effective response,

$$\begin{aligned} \delta\phi^{(n)}_{\rm EFT}(z;\varphi) &= -A^{(n)}n!\sum_k\frac{(k-1)!}{4\pi z^k} \\ &\quad \times [C_{kn}e^{in\varphi} + \chi_{kn}e^{-in\varphi}] + \text{c.c.} \end{aligned} \tag{16}$$

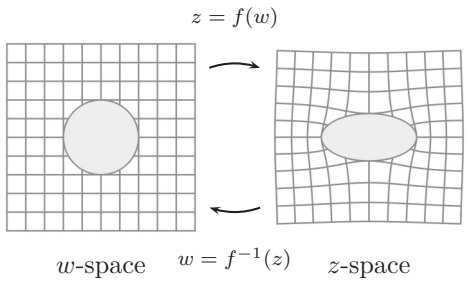

FIG. 3. Conformal mapping between circle (w space) and ellipse (z space) boundaries. The mapping takes a background field $\phi(z)$ imposed on an ellipse to a new field $(\phi\circ f)(w)$ imposed on a circle, for which the response $\delta\phi(w)$ follows from Eq. (18). Mapping back gives the response $(\delta\phi\circ f^{-1})(z)$.

2. *Full theory*

We will first consider the full theory solution for the (BC 2) case and discuss the modifications required for the other boundary conditions shortly after. The full theory response is a solution to the Laplace boundary value problem $\partial\bar\partial\delta\phi = 0$ for the outer domain $z \in \mathbb{R}^2 \setminus \mathcal{A}$, where $\mathcal{A}$ is the area of the ellipse projected onto the base plane, subject to the boundary condition $\phi|_{\partial\mathcal{A}} = (\phi_{\rm bg} + \delta\phi)|_{\partial\mathcal{A}} = \tilde\eta^{(0)}$, where $\tilde\eta^{(0)}$ is the dimensionless free parameter mentioned in Sec. II A describing the height above the base plane, and $\delta\phi \xrightarrow{|z|\to\infty} 0$. Since global height translations are a symmetry of the (BC 2) theory, without loss of generality it suffices to take $\tilde\eta^{(0)} \equiv 0$.

This Dirichlet problem is simple for a circular boundary of radius R. Indeed, for backgrounds that can be put into a Laurent series,

$$\phi(z,\bar z) = \sum_{k>0}\left[a_k\left(\frac{z}{R}\right)^k + b_k\left(\frac{R}{z}\right)^k\right] + \text{c.c.}, \tag{17}$$

the response is given by

$$\delta\phi(z,\bar z) = -\sum_{k>0}\left[(a_k^* + b_k)\left(\frac{R}{z}\right)^k + \text{c.c.}\right], \tag{18}$$

as can be seen by plugging in $z = Re^{i\theta}$. With this in mind, we exploit the conformal symmetry of Laplace's equations and map the ellipse BVP to a circle, solve using the simple replacement, and map back (see Fig. 3).

The conformal transformations between an ellipse (z space) of semimajor axis a and semiminor axis b, with the major axis aligned along the real axis, and a circle (w space) of radius R are

$$z = f(w) = \frac{1}{2}\left(s_+\frac{w}{R} + s_-\frac{R}{w}\right), \tag{19}$$

and

$$w = f^{-1}(z) = \frac{R}{s_+}\left(z + \sqrt{z^2 - s_+s_-}\right), \tag{20}$$

where $s_+ \equiv a + b$ and $s_- \equiv a - b$. The expression for $f^{-1}(z)$ results from solving a quadratic equation, where it is necessary to chose the (+) sign so that the ellipse and circle boundaries correspond. Since we are considering z far outside the ellipse,

the branch cut for the square root can be conveniently chosen as the interval $(-\sqrt{s_+s_-},\sqrt{s_+s_-})$, which lies within the ellipse. Under this transformation, the background field becomes

$$\phi_{\rm bg}^{(n)}(\boldsymbol{w};\varphi)=\frac{A^{(n)}}{2^n}\left[\left(s_+\frac{w}{R}+s_-\frac{R}{w}\right)^n e^{-in\varphi}+\left(s_+\frac{\bar{w}}{R}+s_-\frac{R}{\bar{w}}\right)^n e^{in\varphi}\right]. \tag{21}$$

To solve the circle BVP, we first expand (21) as a binomial series using

$$\left(s_+\frac{w}{R}+s_-\frac{R}{w}\right)^n=\sum_{\ell<n/2}\binom{n}{\ell}s_+^{n-\ell}s_-^{\ell}\left(\frac{w}{R}\right)^{n-2\ell}+\sum_{\ell<n/2}\binom{n}{\ell}s_+^{\ell}s_-^{n-\ell}\left(\frac{R}{w}\right)^{n-2\ell}+\underset{\text{even}}{+}\binom{n}{n/2}(s_+s_-)^{n/2}, \tag{22}$$

where the last term only appears when n is even. This extra constant term can be ignored due to the height-translation symmetry of (BC 2); however, we must revisit it later when we discuss (BC 1). Using (18) we get the response,

$$\delta\phi_{\rm full}^{(n)}(\boldsymbol{w};\varphi)=-\frac{A^{(n)}}{2^n}\sum_{\ell<n/2}\Big[(s_+^{n-\ell}s_-^{\ell}e^{in\varphi} \tag{23}$$

$$+s_+^{\ell}s_-^{n-\ell}e^{-in\varphi})\left(\frac{R}{w}\right)^{n-2\ell}+\text{c.c.}\Big]. \tag{24}$$

To transform back to z space, we set $w=f^{-1}(z)$ and use the expansion,

$$\frac{1}{(1+\sqrt{1-x})^n}=\frac{n}{2^n}\sum_{k=0}^{\infty}\frac{1}{n+2k}\binom{n+2k}{k}\left(\frac{x}{4}\right)^k \tag{25}$$

to give

$$\delta\phi_{\rm full}^{(n)}(\boldsymbol{w};\varphi)=\sum_{\ell<n/2}\sum_{k=0}^{\infty}\mathcal{C}(n,\ell,k)\frac{1}{z^{n-2\ell+2k}}+\text{c.c.}, \tag{26}$$

where

$$\mathcal{C}(n,\ell,k)=-\frac{A^{(n)}}{2^n}\binom{n}{\ell}(s_+^{n-\ell}s_-^{\ell}e^{in\varphi}+s_+^{\ell}s_-^{n-\ell}e^{-in\varphi})\times\left(\frac{s_+}{2}\right)^{n-2\ell}\frac{n-2\ell}{n-2\ell+2k}\binom{n-2\ell+2k}{k}\times\left(\frac{s_+s_-}{4}\right)^k. \tag{27}$$

3. Matching

To match the polarizabilities, we wish to set $\delta\phi_{\rm EFT}^{(n)}\overset{!}{=}\delta\phi_{\rm full}^{(n)}$. So that we can directly compare coefficients, we first put (26) into more convenient form by re-indexing the sums:

$$\delta\phi_{\rm full}^{\binom{n\text{ even}}{n\text{ odd}}}=\sum_{k=\left\{\substack{\text{even}\\\text{odd}}\right\}}^{\infty}\sum_{\ell=\left\{\substack{\text{even}\\\text{odd}}\right\}}^{\min[n,k]}\mathcal{C}\left(n,\frac{n-\ell}{2},\frac{k-\ell}{2}\right)\frac{1}{z^k}+\text{c.c.}, \tag{28}$$

where both sums are over only positive even (odd) integers when n is even (odd). Comparing the coefficients to that of (16) and simplifying finally gives the full set of polarizabilities:

$$C_{nm}=\sum_{\ell=\left\{\substack{\text{even}\\\text{odd}}\right\}}^{\min[n,m]}\frac{4\pi\ell}{2^{n+m}n!m!}\binom{n}{\frac{n-\ell}{2}}\binom{m}{\frac{m-\ell}{2}}(s_+s_-)^{\frac{n+m}{2}}\left(\frac{s_+}{s_-}\right)^{\ell},\quad\left\{\substack{n,m\text{ even}\\n,m\text{ odd}}\right\} \tag{29}$$

$$\chi_{nm}=\sum_{\ell=\left\{\substack{\text{even}\\\text{odd}}\right\}}^{\min[n,m]}\frac{4\pi\ell}{2^{n+m}n!m!}\binom{n}{\frac{n-\ell}{2}}\binom{m}{\frac{m-\ell}{2}}(s_+s_-)^{\frac{n+m}{2}}=\begin{cases}\dfrac{2\pi nm}{2^{n+m}(n+m)}\dfrac{(s_+s_-)^{\frac{n+m}{2}}}{[(\frac{n}{2})!]^2[(\frac{m}{2})!]^2}, & n,m\text{ even}\\[2ex]\dfrac{8\pi}{2^{n+m}(n+m)}\dfrac{(s_+s_-)^{\frac{n+m}{2}}}{[(\frac{n-1}{2})!]^2[(\frac{m-1}{2})!]^2}, & n,m\text{ odd},\end{cases} \tag{30}$$

where we recall that if $n+m\notin 2\mathbb{N}$, then $C_{nm}=\chi_{nm}=0$. This matching procedure gives the polarizabilities for a single ellipse aligned with the x axis, but if we instead consider an ellipse rotated an angle θ from the x axis ($z\to e^{i\theta}z$), then $\partial\to e^{i\theta}\partial$ and it follows that the polarizabilities are modified by

$$C_{nm}\to e^{i(n-m)\theta}C_{nm},\quad \chi_{nm}\to e^{i(n+m)\theta}\chi_{nm}. \tag{31}$$

4. Modifications for other boundary conditions

Although we have only performed the matching for (BC 2), we can also solve for the full set of polarizabilities for (BC 1) and (BC 3) with a few modifications. For the case of (BC 3), the tilt degree of freedom allows the ellipse to align with a dipole background field, so we immediately have that $C_{nm}=\chi_{nm}=0$ if $n=1$ or $m=1$. Since the higher-order multipole fields do not contain tilt, it follows that the remaining polarizabilities are the same as in (BC 3).

For the case of (BC 1), there is no vertical translation symmetry, so we must also include in the effective Hamiltonian the $n=0$ and $m=0$ terms. We will refer to these as *monopole* terms and explicitly distinguish them by writing

$$\beta\Delta\mathcal{H}^M[\phi]=\frac{1}{2}M_0\phi^2(0)+\sum_{\substack{n>0\\\text{even}}}[M_n\phi\partial^n\phi+\bar{M}_n\phi\bar{\partial}^n\phi]_{z=\mathbf{0}}, \tag{32}$$

where $\bar{M}=M^*$ and the condition that n is even follows from the rotation symmetry of the ellipse. These terms present

a particular challenge: the monopole field, proportional to $\log|\boldsymbol{x}|$, exhibits a long-distance divergence and is therefore ill-defined as it stands. For a sensible theory, we must regulate the Hamiltonian so as to dampen the long-range correlations.

Regularization can be realized in a physically motivated way by accounting for the gravitational energy of the surface. The effect is the addition of a small "mass" term into the bulk Hamiltonian[4]:

$$\beta\mathcal{H}_0[\phi] = \frac{1}{2}\int d^2x\left[(\nabla\phi)^2 + \ell_c^{-2}\phi^2\right]. \tag{33}$$

For fluid interfaces with a mass density difference $|\Delta\rho|$, the *capillary length* ℓ_c is given by $\ell_c = \sqrt{\sigma/|\Delta\rho|g}$, where g is the gravitational acceleration. The capillary length is assumed large, so that we have the scaling hierarchy $a,b \ll r = |\boldsymbol{x}| \ll \ell_c$.

With the regulator in place, the bulk Euler-Lagrange equation becomes

$$\left(-\nabla^2 + \ell_c^{-2}\right)\phi = 0. \tag{34}$$

The bulk Green function is then the modified Bessel function of the second kind, which limits to a logarithm for large ℓ_c:

$$G(\boldsymbol{x}) = \frac{1}{2\pi}K_0(r/\ell_c) \xrightarrow{\ell_c\to\infty} -\frac{1}{2\pi}\log\left(\frac{r}{2\ell_c}\gamma_e\right), \tag{35}$$

where $\gamma_e = e^{\gamma_E}$ and γ_E is the Euler-Mascheroni constant.

To match the coefficients, we proceed as before by introducing a background field $\phi_{\rm bg}$, computing the response $\delta\phi^M$ in both the effective and full theories, and comparing. Considering only the monopole terms, the background induces an effective source,

$$J^M(z) = -M_0\delta(z)\phi_{\rm bg}(z) - \sum_{\substack{n>0\\ \text{even}}}\left[M_n(\delta(z)\partial^n\phi_{\rm bg}(z) + (-1)^n\partial^n[\delta(z)\phi_{\rm bg}(z)]) + \text{c.c.}\right]. \tag{36}$$

Convolving with the bulk Green function gives effective linear response,

$$\delta\phi^M(z) = -M_0G(z)\phi_{\rm bg}(0) - \sum_{\substack{n>0\\ \text{even}}}\left[M_n(G(z)\partial^n\phi_{\rm bg}(0) + (-1)^n\partial^nG(z)\phi_{\rm bg}(0)) + \text{c.c.}\right]. \tag{37}$$

Using the asymptotic form of the Green function, the final result is

$$\delta\phi^M(z) = \frac{M_0}{2\pi}\log\left(\frac{|z|\gamma_e}{2\ell_c}\right)\phi_{\rm bg}(0) - \sum_{\substack{n>0\\ \text{even}}}\left\{M_n\left[-\frac{1}{2\pi}\log\left(\frac{|z|\gamma_e}{2\ell_c}\right)\partial^n\phi_{\rm bg}(0) + \frac{1}{4\pi}\frac{(n-1)!}{z^n}\phi_{\rm bg}(0)\right] + \text{c.c.}\right\}. \tag{38}$$

Since the bulk Hamiltonian with the "mass" term is no longer conformal, we unfortunately cannot use the mapping trick as before to compute the full-theory response. However, based on the geometry of the system, it will prove convenient to work in confocal elliptic coordinates, defined by

$$x = f\cosh\xi\cos\eta, \quad y = f\sinh\xi\sin\eta, \tag{39}$$

where $\xi\in[0,\infty)$, $\eta\in(-\pi,\pi]$, and the focus $f = \sqrt{a^2-b^2}$. Curves of constant ξ give ellipses, as can be seen by rearranging the defining equations:

$$\left(\frac{x}{f\cosh\xi}\right)^2 + \left(\frac{y}{f\sinh\xi}\right)^2 = \cos^2\eta + \sin^2\eta = 1.$$

In particular, the boundary of our ellipse results from setting $f\cosh\xi_0 = a$ and $f\sinh\xi_0 = b$, which leads to

$$fe^{\pm\xi_0} = a\pm b \Rightarrow \xi_0 = \frac{1}{2}\log\left(\frac{a+b}{a-b}\right). \tag{40}$$

In complex variables, the defining relations (39) can be written simply as

$$z = f\cosh(\xi + i\eta). \tag{41}$$

To extract ξ we must invert the hyperbolic cosine. From the definition of cosh, we find

$$fe^{\xi+i\eta} = z \pm \sqrt{z^2-f^2}. \tag{42}$$

The sign ambiguity is resolved by defining the branch cuts of the multivalued square root as before and requiring the ellipse boundary to be consistent. Just as in Eq. (20), we take the (+) sign. Consistency is checked by evaluating (42) at any point (ξ_0,η) on the boundary, for which the left side gives

$$fe^{\xi_0+i\eta} = (a+b)e^{i\eta}.$$

The set of solutions for the full theory is found in Appendix A. Using the $n=0$ background field of Eq. (B5), for which $\phi_{\rm bg}^{(0)} = A^{(0)}$ and $\partial^n\phi_{\rm bg}^{(0)}(0) = 0$, the full-theory response is

$$\delta\phi_{\rm full} = -A^{(0)}\frac{\log\left(\frac{fe^{\xi}}{4\ell_c}\gamma_e\right)}{\log\left(\frac{a+b}{4\ell_c}\gamma_e\right)}. \tag{43}$$

To proceed, we must express (43) in complex variables. This is accomplished by first noting that

$$e^{2\xi} = \left|z/f + \sqrt{(z/f)^2-1}\right|^2, \tag{44}$$

which follows from multiplying Eq. (42) by its complex conjugate, and then expanding the logarithm of (43) for

[4]Note that this change in the bulk Hamiltonian *does not* alter our effective worldline Hamiltonian. The appearance of $\partial\bar\partial\phi$ in any operator can be traded for $\ell_c^{-2}\phi$ by the bulk Euler-Lagrange equation (34), and can therefore be absorbed into one of the preexisting terms.

large z:

$$\log\left(\frac{f e^{\xi}\gamma_e}{4\ell_c}\right) = \frac{1}{2}\log\left(\frac{f^2 e^{2\xi}\gamma_e^2}{16\ell_c^2}\right)$$
$$= \frac{1}{2}\log\left(\left|\frac{z\gamma_e}{4\ell_c}\right|^2 \left|1+\sqrt{1-(f/z)^2}\right|^2\right)$$
$$= \log\left(\frac{|z|\gamma_e}{2\ell_c}\right) - \frac{1}{2}\sum_{\substack{n>0\\ \text{even}}} \frac{(n-1)!}{2^n\left[\left(\frac{n}{2}\right)!\right]^2}$$
$$\times\left[\left(\frac{f}{z}\right)^n + \left(\frac{f}{\bar{z}}\right)^n\right]. \tag{45}$$

Plugging this into (43) and comparing to (38) yields the monopole polarizabilities,

$$M_n = \frac{2\pi}{2^n\left[\left(\frac{n}{2}\right)!\right]^2}\frac{(a^2-b^2)^{n/2}}{\log\left(\frac{4\ell_c}{(a+b)\gamma_e}\right)}. \tag{46}$$

For an ellipse rotated an angle θ from the x axis, the polarizability $M_n \to e^{in\theta}M_n$.

Since the bulk Hamiltonian has been modified, the question arises as to whether the higher-order polarizabilities will be affected. At first glance, it appears they may be unaltered since the higher-order terms are conformal and the associated effective response involves only derivatives of the Green function, which are nonsingular in the $\ell_c \to \infty$ limit. But, due to the boundary conditions we cannot ignore the constant term generated in (22). However, this term behaves like the constant background field introduced above and, as shown in Appendix C, the monopole terms conspire to exactly cancel it, thereby leaving C_{nm}, χ_{nm}, and $\bar{\chi}_{nm}$ with the same values found for (BC 2).

5. *Rods and disks*

The polarizabilities of thin rods and disks are natural limiting cases of our ellipse model. For a thin rod of length L, the full set of polarizabilities is given by (29), (30), and (46)—with subsets vanishing depending on the boundary conditions—with $a \to L/2$ and $b \to 0$ ($s_\pm \to L/2$), which does not change the overall form of the equations. However, for a rotationally symmetric disk we expect the anisotropic terms to vanish. Indeed, setting $a,b \to R$ ($s_+ \to 2R, s_- \to 0$) gives $\chi = \bar{\chi} = 0$. For C_{nm}, the only nonvanishing terms are those for which $\ell = (n+m)/2$. Since $\ell \leqslant \min[n,m]$, taking $n \geqslant m$ leads to $(n+m)/2 \leqslant m \Rightarrow n \leqslant m$, therefore $n = m$. Hence, for disks,

$$C_{nm} = \frac{4\pi R^{2n}}{n!(n-1)!}\delta_{nm}, \tag{47}$$

which agrees with [13] and [17] up to a factor of 2^{-n} due to the difference in definition. Additionally, the only surviving monopole term is

$$M_0 = \frac{2\pi}{\log\left(\frac{2\ell_c}{R\gamma_e}\right)},$$

in agreement with [13] up to normalization.

IV. INTERACTIONS

As mentioned previously, the interaction potentials appear in the free energy $\mathcal{F}$ in (3). In particular, we can write the interaction potential $\mathcal{U}$ as the difference in the free energy with respect to the particle-free surface,

$$-\beta\mathcal{U} = -\beta(\mathcal{F}-\mathcal{F}_0) = \log(Z/Z_0)$$
$$= \sum_{k=0}^{\infty}\frac{1}{k!}\langle(-\beta\Delta\mathcal{H}[\phi])^k\rangle_c, \tag{48}$$

where Z_0 is the free (bulk) partition function ($\Delta\mathcal{H} = 0$), the correlation functions are (Gaussian) averages over the free Hamiltonian,

$$\langle\mathcal{O}\rangle = \frac{1}{Z_0}\int \mathcal{D}\phi\,\mathcal{O}\,e^{-\beta\mathcal{H}_0[\phi]}, \tag{49}$$

and the sum is over all *connected* correlation functions (i.e., cumulants).

Equation (48) can be recast in terms of Feynman diagrams using the standard rules. Since the Hamiltonian is strictly quadratic in ϕ, we assign to each vertex and line, respectively,

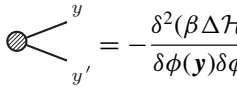

$$= -\frac{\delta^2(\beta\Delta\mathcal{H}[\phi])}{\delta\phi(\boldsymbol{y})\delta\phi(\boldsymbol{y}')}, \quad x \text{ —— } y = G(\boldsymbol{x},\boldsymbol{y}).$$

Each diagram is calculated by integrating over all internal points and dividing by the symmetry factor (the order of the diagram's group of automorphisms). Equation (48) is then recognized as the sum of all connected bubble diagrams, which in our case consists of diagrams with the topology of a ring. A ring of k vertices possess the symmetries of the dihedral group D_k (k rotations and k reflections), so the symmetry factor is simply $|D_k| = 2k$. Equation (48) is therefore given by[5]

$$-\beta\mathcal{U} = \sum_{k=1}^{\infty}$$
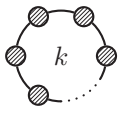

$$= \sum_{k=1}^{\infty}\frac{1}{2k}\,\mathrm{Tr}\left(-\int \mathrm{d}^2y'\,G(\boldsymbol{x},\boldsymbol{y}')\frac{\delta^2(\beta\Delta\mathcal{H})}{\delta\phi(\boldsymbol{y}')\delta\phi(\boldsymbol{y})}\right)^k. \tag{50}$$

To add a bit more physical intuition to the diagrams, we can also explicitly expand the vertices over the particle *worldlines* (particle positions) in the same manner as Refs. [12,13]:

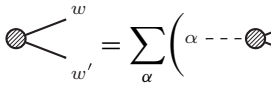

$$= \sum_{\alpha}\left(\alpha \text{ - - - }\right). \tag{51}$$

In this way, the particle interactions become more transparent as exchanges of capillary wave excitations which "propagate"

[5]The functional trace is defined analogously to a matrix trace, but the repeated arguments are integrated over:

$$\mathrm{Tr}[K(\boldsymbol{x},\boldsymbol{y})]^n = \int d^2x_1\cdots d^2x_n\prod_{i=1}^{n}K(\boldsymbol{x}_i,\boldsymbol{x}_{i+1}),$$

where $\boldsymbol{x}_{n+1} = \boldsymbol{x}_1$.

between each particle's respective worldline, as illustrated in the following $k = 4$ diagram for two particles located at $\boldsymbol{x}_1$ and $\boldsymbol{x}_2$, respectively:

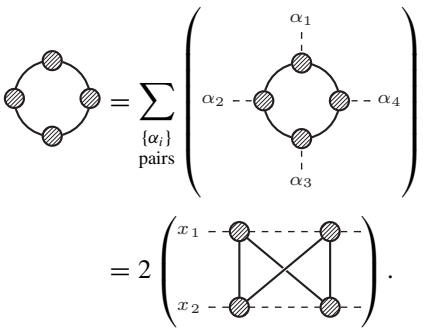

In what follows, we will forgo the explicit diagrammatic expansion over particle worldlines for the sake of brevity, instead containing the sum within the vertices.

To make headway in our calculations, we need to examine all the terms contained within the vertex. For the moment, we will ignore the monopole terms and relegate their discussion to Sec. V.

If we were to calculate the functional derivatives and expand (50), or equivalently perform the Wick contractions in (48), we would encounter the following terms:

$$\left\langle \partial^n_{z_\alpha} \phi(z_\alpha) \partial^m_{z_\beta} \phi(z_\beta) \right\rangle = \partial^n_{z_\alpha} \partial^m_{z_\beta} G^{\alpha\beta}, \tag{52a}$$

$$\left\langle \bar\partial^n_{z_\alpha} \phi(z_\alpha) \bar\partial^m_{z_\beta} \phi(z_\beta) \right\rangle = \bar\partial^n_{z_\alpha} \bar\partial^m_{z_\beta} G^{\alpha\beta}, \tag{52b}$$

$$\left\langle \partial^n_{z_\alpha} \phi(z_\alpha) \bar\partial^m_{z_\beta} \phi(z_\beta) \right\rangle = \partial^n_{z_\alpha} \bar\partial^m_{z_\beta} G^{\alpha\beta}, \tag{52c}$$

where $G^{\alpha\beta} \equiv G(z_\alpha - z_\beta)$. For interactions on the same particle worldline, $z_\alpha = z_\beta$, all three terms diverge and require a renormalization treatment. These "self-interaction" divergences, however, are all powerlike and can therefore be removed by pure counterterms—a reflection that these divergences contain no physical information. As a result, we can safely set to zero any diagram that contains self-interactions. In terms of diagrammar, a vertex assigned to particle α cannot connect to another vertex assigned to α. For more details, see [13].

If we instead consider $z_\alpha \neq z_\beta$, all three terms of (52) are regular, but we notice that $(52c) = 0$ as expected from the Euler-Lagrange equation. We can make this relation manifest diagrammatically by expanding the vertex in the following way:

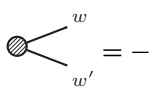

$$= -\sum_\alpha \sum_{n,m\geqslant 1} \Big\{ C^\alpha_{nm} \partial^n_{z_\alpha} \delta^{z_\alpha}_w \bar\partial^m_{z_\alpha} \delta^{z_\alpha}_{w'} + \frac{1}{2} \chi^\alpha_{nm} \partial^n_{z_\alpha} \delta^{z_\alpha}_w \partial^m_{z_\alpha} \delta^{z_\alpha}_{w'} + \frac{1}{2} \bar\chi^\alpha_{nm} \bar\partial^n_{z_\alpha} \delta^{z_\alpha}_w \bar\partial^m_{z_\alpha} \delta^{z_\alpha}_{w'} + (w \leftrightarrow w') \Big\}$$

$$\equiv$$

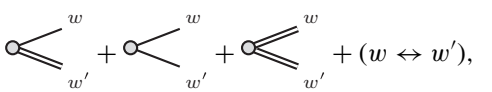

$$+ (w \leftrightarrow w'), \tag{53}$$

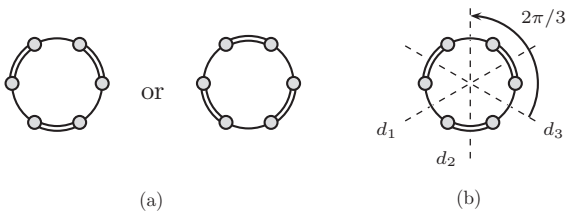

FIG. 4. Two distinct orientations of a $k = 6$ diagram are shown in (a). The weight of the diagram is then $2/(2 \times 6) = 1/6$. The group of diagram automorphisms consist of the identity, two rotations by $2\pi/3$, and three reflections about the lines d_1, d_2, and d_3 as shown in (b). The symmetry factor of the diagram is then $S_\Gamma = 1 + 2 + 3 = 6$. The weight of the diagram is then $1/S_\Gamma = 1/6$, in agreement with the previous argument.

where $\delta^z_w \equiv \delta(z - \boldsymbol{w})$. The single and double lines indicate how to connect the various vertices to ensure each diagram is nonvanishing.

Calculating the free energy then consists of expanding the vertices for each diagram of (50) according to (53), at which point the number of diagrams quickly proliferates. We can group the diagrams by noting that two diagrams are equivalent if they can be reflected or rotated into one another. Under this grouping, each representative diagram then carries an extra factor given by the number of distinct orientations multiplied by a factor of 2 for each χ and $\bar\chi$ vertices, due to the symmetry of their indices. The powers of 2 are canceled by the factors of $1/2$ in (53). What remains simplifies to the expected $1/S_\Gamma$, where $S_\Gamma = |\,\mathrm{Aut}(\Gamma)|$ is the symmetry factor for the diagram Γ. For an example, see Fig. 4. The number of expected diagrams with k vertices is equivalent to the standard combinatorial problem of the number of ways to paint a necklace of k beads with only two colors. However, relationships among the diagrams effectively reduce this number; exchanging single lines and double lines gives the complex conjugate of the diagram. Diagrams with equal numbers of single line and double line edges, which can only occur for those with an even number of vertices, give diagrams in the same equivalency class of the original under this exchange (they are related by reflections and rotations) and therefore are their own conjugate; i.e., they are real.

To illustrate the diagrammatic rules, we calculate an example $k = 4$ diagram. After assigning dummy particle labels and indices to each vertex, we write down the product of vertex factors and Green functions, sum over all labels and indices, and divide by the symmetry factor:

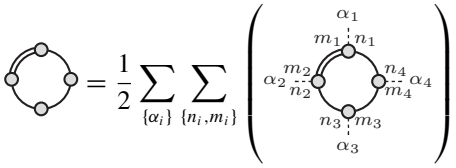

$$= \frac{1}{2} \sum_{\{\alpha_i\}} \sum_{\{n_i, m_i\}} C^{\alpha_1}_{n_1 m_1} C^{\alpha_2}_{n_2 m_2} \chi^{\alpha_3}_{n_3 m_3} \chi^{\alpha_4}_{n_4 m_4} \times \bar G^{m_1 m_2}_{\alpha_1 \alpha_2} G^{n_2 n_3}_{\alpha_2 \alpha_3} G^{m_3 m_4}_{\alpha_3 \alpha_4} G^{n_4 n_1}_{\alpha_4 \alpha_1},$$

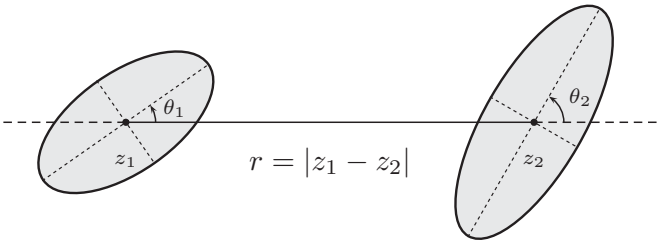

FIG. 5. Configuration for two ellipses as viewed from above.

where we have used the abbreviated notation,

$$G^{n_i n_j}_{\alpha_i \alpha_j} \equiv \partial^{n_i}_{\alpha_i} \partial^{n_j}_{\alpha_j} G^{\alpha_i \alpha_j}, \quad \bar{G}^{n_i n_j}_{\alpha_i \alpha_j} \equiv \bar{\partial}^{n_i}_{\alpha_i} \bar{\partial}^{n_j}_{\alpha_j} G^{\alpha_i \alpha_j}.$$

A. Pair interactions

1. Interaction energies

Consider two ellipses of semimajor axes a_1, a_2 and semiminor axes b_1, b_2, respectively, positioned and oriented as shown in Fig. 5. The interaction energy expansion will only contain diagrams with an even number of vertices to prevent self-interactions once the particle assignments are made at each vertex. We provide explicitly the relevant diagrams and their corresponding symmetry factors in Fig. 6 for reference. To order the expansion in powers of r, we note that each vertex places derivatives on the propagators (Green functions), and $\partial^n G \sim r^{-n}$ [as per Eq. (15)]. It follows that each diagram with a set of vertex indices $\{n_i, m_i\}$ will be of the order $r^{-\sum_i (n_i + m_i)}$. Determining which diagrams are relevant at $O(r^{-p})$ is therefore equivalent to the problem of partitioning the integer p into $2k$ integers and distributing them across the index pairs $\{n_i, m_i\}_{i \leqslant k}$ at each of the k vertices (while satisfying our constraint that $n_i + m_i \in 2\mathbb{N}$). The resulting interaction energy can then be written in the form,

$$-\beta \mathcal{U} = \sum_{\substack{p>0 \\ \text{even}}} \frac{u^{(p)}}{r^p}. \tag{54}$$

The leading-order terms come from the $k = 2$ diagrams. For (BC 2), the polarizabilities begin at $n = m = 1$ and hence the leading-order interaction energy is $O(r^{-4})$. For (BC 3), however, these coefficients vanish and the polarizabilities begin at $n = m = 2$, implying the leading-order interaction energy is $O(r^{-8})$. Following the diagrammatic rules and accounting for the angular dependence using (31), we calculate the diagrams in Fig. 6 and find for (BC 2):

$$u^{(4)} = \frac{1}{16}\left[(s_1^+ s_2^+)^2 + f_1^2 f_2^2 \cos(2\theta_1 + 2\theta_2)\right], \tag{55}$$

$$u^{(6)} = \frac{1}{32}\Big\{(s_1^+ s_2^+)^2\left[(s_1^+)^2 + 3 f_1^2 \cos(2\theta_1)\right] + 4 f_1^4 f_2^2 \cos(4\theta_1 + 2\theta_2)\Big\} + (1 \leftrightarrow 2), \tag{56}$$

$$u^{(8)} = \frac{1}{2^{10}}\Big\{19(s_1^+ s_2^+)^4 + f_1^2 f_2^2 (s_1^+ s_2^+)^2 [36\cos(2\theta_1 - 2\theta_2) + 124\cos(2\theta_1 + 2\theta_2)] + 271 f_1^4 f_2^4 \cos(4\theta_1 + 4\theta_2) + 12(s_1^+)^6 (s_2^+)^2 + 36 f_1^4 (s_1^+ s_2^+)^2 + 2 f_1^4 (s_2^+)^4 + 32(s_1^+ s_2^+)^2 f_1^2 [2(s_1^+)^2 + 3(s_2^+)^2]\cos(2\theta_1) + 80 f_1^4 (s_1^+ s_2^+)^2 \cos(4\theta_1) + 192 f_1^6 f_2^2 \cos(6\theta_1 + 2\theta_2)\Big\} + (1 \leftrightarrow 2), \tag{57}$$

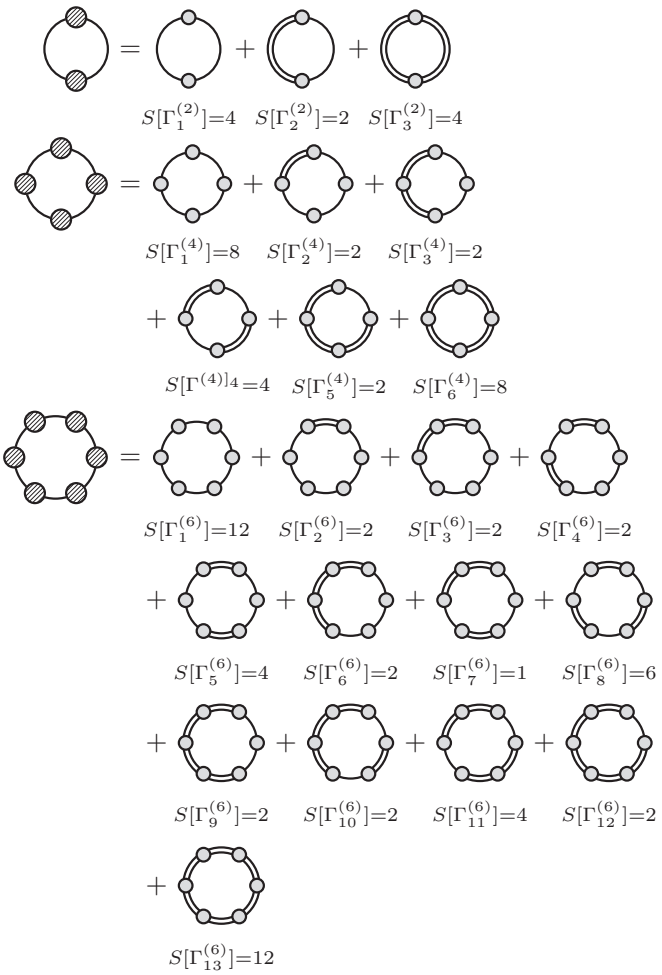

FIG. 6. Relevant diagram expansions for pair interactions up to $k = 6$ vertices, complete with symmetry factors. Note that diagrams containing a nonequal number of single line to double line edges have complex conjugate partners. In particular, we have $\Gamma_3^{(2)} = (\Gamma_1^{(2)})^*$, $\Gamma_6^{(4)} + \Gamma_5^{(4)} = (\Gamma_1^{(4)} + \Gamma_2^{(4)})^*$, and $\Gamma_{13}^{(6)} + \Gamma_{12}^{(6)} + \Gamma_{11}^{(6)} + \Gamma_{10}^{(6)} + \Gamma_9^{(6)} = (\Gamma_1^{(6)} + \Gamma_2^{(6)} + \Gamma_3^{(6)} + \Gamma_4^{(6)} + \Gamma_5^{(6)})^*$.

where $f^2 = s_+ s_-$ as before. Since the expressions become increasingly more lengthy, we have only included the interactions up to and including $O(r^{-10})$, which only require diagrams with $k = 2$ and $k = 4$ vertices. The $k = 6$ diagrams appear at $O(r^{-12})$.

For (BC 3) we find

$$u^{(8)} = \frac{9}{256}\left[(s_1^+ s_2^+)^4 + f_1^4 f_2^4 \cos(4\theta_1 + 4\theta_2)\right], \tag{58}$$

$$u^{(10)} = \frac{3}{128}\left[(s_1^+)^6 (s_2^+)^4 + 5 f_1^2 (s_1^+ s_2^+)^4 \cos(2\theta_1) + 3 f_1^4 (s_1^+)^2 (s_2^+)^4 + 9 f_1^6 f_2^4 \cos(6\theta_1 + 4\theta_2)\right] + (1 \leftrightarrow 2), \tag{59}$$

$$u^{(12)} = \frac{5}{2^{11}}\{5(s_1^+ s_2^+)^6 + 45(s_1^+ s_2^+)^2 f_1^4 f_2^4 + 4(s_1^+ s_2^+)^4 f_1^2 f_2^2 \times [10\cos(2\theta_1 - 2\theta_2) + 21\cos(2\theta_1 + 2\theta_2)] + 396 f_1^6 f_2^6 \cos(6\theta_1 + 6\theta_2) + 5(s_1^+ s_2^+)^2 [(s_1^+)^6 (s_2^+)^2 + 6(s_1^+)^4 f_2^4 + 8(s_1^+ s_2^+)^2 f_2^4] + 12(s_1^+ s_2^+)^2 f_1^2 \cos(2\theta_1) \times [3(s_1^+)^4 (s_2^+)^2 + 4(s_1^+)^2 (s_2^+)^4 + 6 f_1^4 (s_2^+)^2 + 12(s_1^+)^2 f_2^4] + 63(s_1^+ s_2^+)^4 f_1^4 \cos(4\theta_1) + 216 f_1^8 f_2^4 \cos(8\theta_1 + 4\theta_2)\} + (1 \leftrightarrow 2). \quad (60)$$

To this order, only the diagrams with $k = 2$ vertices contribute. The $k = 4$ diagrams do not contribute until $O(r^{-16})$.

For identical ellipses, we simply set $s_1^\pm = s_2^\pm$ in the above expressions. The leading-order terms then reproduce the results of [8] up to powers of 2^p for $O(r^{-p})$, where the discrepancy is due to differing assignments of a and b ([8] refers to the principal axes, which are twice the values of the semimajor and semiminor axes used here). Setting $s_i^+ = 2R_i$ and $s_i^- = 0$ gives the interaction energy between two disks of radii R_1 and R_2, respectively, and reproduce the results of [13] for (BC 2). Since the expression for disks obeying (BC 3) appears to be absent from the literature, we provide the first few terms explicitly:

$$\beta\mathcal{U} = -9\frac{R_1^4 R_2^4}{r^8} - 24\frac{R_1^6 R_2^4 + R_1^4 R_2^6}{r^{10}} - 50\frac{R_1^8 R_2^4 + 2R_1^6 R_2^6 + R_1^4 R_2^8}{r^{12}} + \cdots \quad (61)$$

Furthermore, setting $s_i^\pm = L_i/2$ in Eqs. (57) and (60) gives the interaction energy between rods.

Since we have computed the interaction energies between nonidentical ellipses, we can also consider the limiting cases of disks and rods for each particle independently. Doing so gives new results for the interactions between an ellipse and rod, ellipse and disk, and a rod and disk. Furthermore, since the boundary constraints are contained within the polarizabilities, it is straightforward to compute the interactions between particles with different boundary conditions. For example, the leading-order interactions between a bobbing disk and an ellipse free to bob and tilt is given by the polarizabilities C_{11}^D and C_{22}^E for the disk and ellipse, respectively, yielding

$$\beta\mathcal{U} = -\frac{R^2(a+b)^4}{16r^6} + O(r^{-8}). \quad (62)$$

2. Orientational dependence

At leading order for (BC 2), the energy is minimized for $\theta_1 + \theta_2 = n\pi$, $n \in \mathbb{Z}$, which is degenerate for a full range of angles. Similarly, there is a degenerate maximum energy state given by $\theta_1 + \theta_2 = (n + 1/2)\pi$, $n \in \mathbb{Z}$. This degeneracy was noted in Ref. [11] with the speculation that it should be broken by higher-order terms. Indeed, at the very next order, the angular dependence breaks this symmetry and we find the true minimum energy configuration occurs for $\theta_1 = \theta_2 = 0$ (up to integer multiples of π) which aligns the major principal axes (tip-to-tip). The energy is maximized for two unique values $\theta_1 = \theta_2 \lesssim \pi/4$ and $\gtrsim 3\pi/4$ which depend on particle size and separation. This symmetry breaking is illustrated in Fig. 7 for the limiting case of identical rods. Although the leading-order angular dependence for (BC 3) differs by an additional factor of two from (BC 2), we find similar behavior, but the least-preferred orientations—which depend on particle size and separation—lie within the intervals $(\pi/4,\pi/2)$ and $(\pi/2,3\pi/4)$. It is interesting to compare the preferred orientations with those observed for ellipsoidal objects in the three-dimensional electromagnetic case [25]—the preferred orientations are similar, but the least preferred orientations are different.

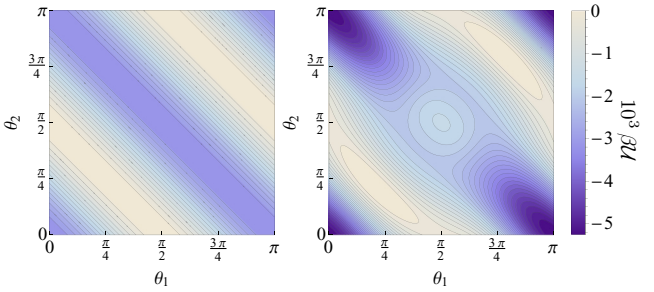

FIG. 7. (Color online) Plots of the pair interaction free energy between identical rods of length L separated by a distance $r = 1.25L$. The leading-order $O(r^{-4})$ result is shown on the left, while the right plot includes the $O(r^{-6})$ correction.

B. Multibody interactions

In addition to pairwise interactions, the energy also receives contributions from multibody terms. In general, N-body interactions will begin to appear in diagrams with N vertices of lowest multipole order. However, in special cases the symmetry of the particles may lead to the vanishing of some terms. In particular, for axisymmetric particles (disks), only the C_{nn} polarizabilities are nonzero and all diagrams with an odd number of vertices vanish. This is obvious diagrammatically, since it is impossible to connect an odd number of C vertices such that each vertex possesses both a single and double line. This property was first stated in Ref. [13] (with slightly different diagrammatic rules), and simply reflects the vanishing of $\partial\bar{\partial}G$. With this symmetry relaxed, however, the χ vertices allow for nonvanishing diagrams with an odd number of vertices and represent pure anisotropic effects. For brevity, we will restrict our discussion to the (BC 2) case, but the results for (BC 3) will follow similarly.

Since the multibody interactions mix the particle coordinates, it is desirable to define a suitable parametrization that relates to the geometry of the particle configuration in a coordinate-free manner. To this aim, we define $z_{ij} \equiv z_j - z_i \equiv r_{ij}e^{i\varphi_{ij}}$ as well as the exterior vertex angle $\varphi_{ik}^j \equiv -\varphi_{ij} + \varphi_{jk}$ as shown in Fig. 8. Furthermore, we parametrize the orientation of the particles with respect to the exterior vertex angles via $\theta_{ij}^{(j)} \equiv \theta_j - \varphi_{ij}$, where θ_i is the angle the particle makes from the x axis. Note that $\varphi_{ji} \equiv \varphi_{ij} \pmod{\pi}$, and therefore under the exchange of indices we can equate $\varphi_{ki}^j = -\varphi_{ik}^j$ and $\theta_{ij}^{(i)} = \theta_{ji}^{(i)}$ up to integer multiples of π.

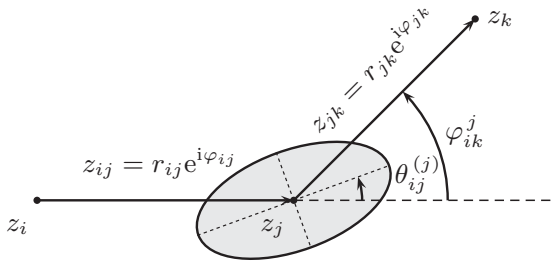

FIG. 8. An illustration of the angle definitions for a particle at position z_j.

We first consider the leading-order triplet (three-body) interaction, which comes from the diagrams,

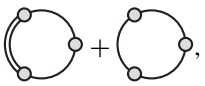

(63)

and their complex conjugates. Since self-interactions are set to zero, the sum over particle labels becomes the sum over permutations of {1,2,3}. Computing the diagrams results in

$$\beta\mathcal{U}^{(6)}_{\{1,2,3\}} = -\frac{1}{64}\sum_{i,j,k}^{\substack{\text{perm.}\\ \{1,2,3\}}} \frac{1}{r_{ij}^2 r_{jk}^2 r_{ki}^2}\left\{\frac{1}{3} f_i^2 f_j^2 f_k^2 \times \cos\left[2\left(\theta^{(i)}_{ki} + \theta^{(j)}_{ij} + \theta^{(k)}_{jk}\right)\right] + f_i^2 (s_j^+ s_k^+)^2 \cos\left[2\left(\theta^{(i)}_{ki} + \varphi^j_{ik}\right)\right]\right\}. \quad (64)$$

This expression can be simplified by noting that the sum can be split into the sum over even and odd cyclic permutations. If the summand is invariant under the exchange of two indices, the sum can be written as twice the sum over cyclic permutations. The second term is seen to be invariant under $j \leftrightarrow k$ by noticing that

$$\begin{aligned}\theta^{(i)}_{ji} + \varphi^k_{ij} &= \theta_i - \varphi_{ji} - \varphi_{ik} + \varphi_{kj} \\ &= \theta^{(i)}_{ki} + \varphi^j_{ik}.\end{aligned}$$

Using this same property, we see the first term is also invariant under $j \leftrightarrow k$:

$$\begin{aligned}\theta^{(i)}_{ji} + \theta^{(k)}_{ik} + \theta^{(j)}_{kj} &= \theta^{(i)}_{ki} + \theta^{(j)}_{ij} + \theta^{(k)}_{jk} - \varphi^j_{ik} - \varphi^k_{ji} - \varphi^i_{kj} \\ &= \theta^{(i)}_{ki} + \theta^{(j)}_{ij} + \theta^{(k)}_{jk} - 2\pi,\end{aligned}$$

where we have used that the sum over all external angles gives 2π. The result finally simplifies to

$$\beta\mathcal{U}^{(6)}_{\{1,2,3\}} = -\frac{1}{32}\frac{1}{r_{12}^2 r_{23}^2 r_{31}^2}\left\{f_1^2 f_2^2 f_3^2 \times \cos\left[2\left(\theta^{(1)}_{31} + \theta^{(2)}_{12} + \theta^{(3)}_{23}\right)\right] + \sum_{i,j,k}^{\substack{\text{cyc.}\\ \{1,2,3\}}} f_i^2 (s_j^+ s_k^+)^2 \cos\left[2\left(\theta^{(i)}_{ki} + \varphi^j_{ik}\right)\right]\right\}. \quad (65)$$

From the above expression, we see that the minimum energy configurations—suggested from the triplet interaction alone—occur for $\theta^{(i)}_{ki} = -\varphi^j_{ik}$, up to integer multiples of π. It is also apparent that the least preferred configurations occur when $\theta^{(i)}_{ki} = \pi/2 - \varphi^j_{ik}$, which maximizes the energy. Note that we can as well rewrite these expressions in terms of the *interior* angles by noting that an interior angle $\alpha^j_{ik} = \pi - \varphi^j_{ik}$, but all expressions are equivalent modulo π. These configurations are illustrated in Fig. 9.

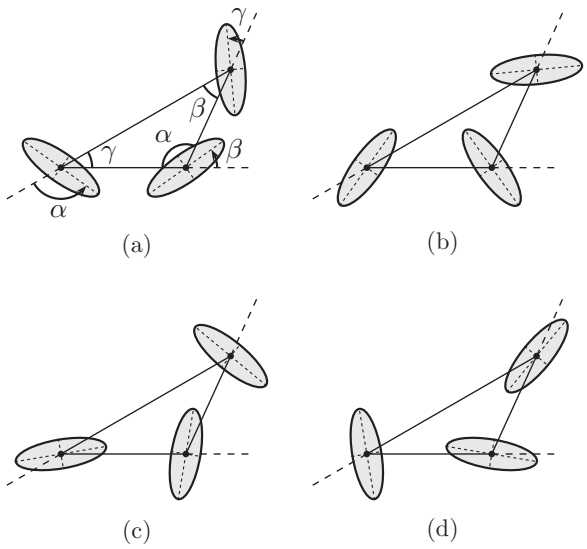

FIG. 9. Illustration of the various ellipse orientations for an arbitrary three-body particle configuration. The pure triplet interaction suggests configuration (a) is preferred (minimizes the energy), while configuration (b) is preferred the least (maximizes the energy). However, with the inclusion of all the pair interactions up to the same order, this conclusion switches: (b) is actually preferred, while (a) is just a local minimum. The least preferred configurations as suggested by the pair interactions are shown in (c) and (d).

Since pair interactions will of course also contribute to the three-body interaction energy, it may be that the preferred angular configuration suggested above could be modified. From the leading-order pair interaction Eq. (55), we find

$$\beta\mathcal{U}^{(4)}_p = -\frac{1}{16}\sum_{i,j,k}^{\substack{\text{cyc.}\\ \{1,2,3\}}} \frac{1}{r_{ij}^4}\left\{(s_i^+ s_j^+)^2 + f_i^2 f_j^2 \cos\left[2\left(\theta^{(i)}_{ki} + \theta^{(j)}_{ij} - \varphi^i_{kj}\right)\right]\right\}. \quad (66)$$

The energy is minimized when

$$\theta^{(i)}_{ki} + \theta^{(j)}_{ij} - \varphi^i_{kj} \equiv 0 \pmod{\pi}.$$

Solving this system of equations gives the solution,

$$\theta^{(i)}_{ki} = \pi - \varphi^j_{ik} + \frac{n\pi}{2} = \alpha^j_{ik} + \frac{n\pi}{2},\ n \in \mathbb{Z}. \quad (67)$$

The angular configuration that maximizes the energy is similar, but with $\pi/4$ subtracted from each angle. These configurations again appear in Fig. 9.

At leading order, the interaction energy therefore suffers from a double degeneracy. This degeneracy is broken at the next order with the pair and triplet interactions. To simplify the remainder of our discussion, we can take advantage of the similarity of the solutions—the preferred ellipse

orientations all depend similarly on the respective adjacent interior angles of the particle configuration—and consider the highly symmetric case of the particles sitting at the vertices of an equilateral triangle with side lengths d. Furthermore, consider the limiting case in which the ellipses become identical rods of length L. This results in reducing the problem to a one-dimensional angular subspace in which $\theta_{ki}^{(i)} = \theta$ for each rod. This simplification gives for the pair energies,

$$\beta\mathcal{U}_p^{(4)} = -\frac{3}{16}\left(\frac{L}{2d}\right)^4\left\{1+\cos\left[4\left(\theta-\frac{\pi}{3}\right)\right]\right\}, \tag{68}$$

$$\beta\mathcal{U}_p^{(6)} = -\frac{3}{32}\left(\frac{L}{2d}\right)^6\left\{2+3\cos\left[2\left(\theta-\frac{2\pi}{3}\right)\right]+3\cos(2\theta) +4\cos\left[2\left(3\theta-\frac{4\pi}{3}\right)\right]+4\cos\left[2\left(3\theta-\frac{2\pi}{3}\right)\right]\right\}; \tag{69}$$

and for the triplet energy,

$$\beta\mathcal{U}_t^{(6)} = -\frac{1}{32}\left(\frac{L}{2d}\right)^6\left\{\cos(6\theta)+3\cos\left[2\left(\theta+\frac{2\pi}{3}\right)\right]\right\}. \tag{70}$$

The result, which is plotted in Fig. 10, is that the degeneracy is broken, with the $\theta = 5\pi/6$ configuration preferred. This implies the $\theta_{ki}^{(i)} = \alpha_{ik}^{j} + \pi/2$ solution from before is the true minimum. Surprisingly, there is a competition at $O(d^{-6})$ between the pairs and triplet: The preferred angular configurations are opposite one another, but with the pairs ultimately dominating. That is, the triplet interaction alone suggests the opposite conclusion of the full result, and simply decreases the difference between the two minima.

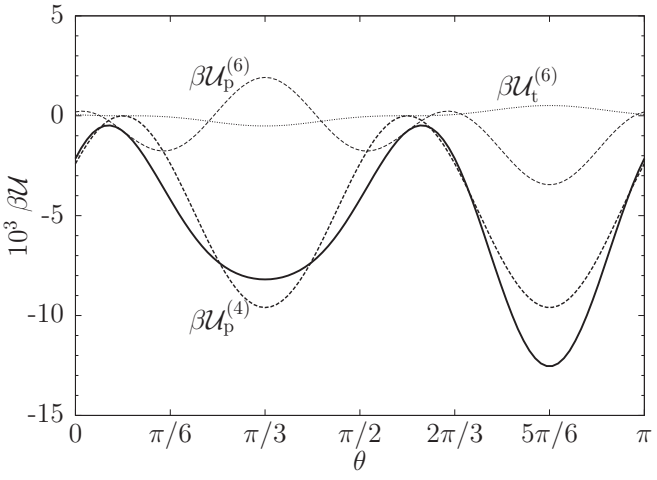

FIG. 10. Plot of the pair and triplet contributions to the overall interaction free energy for identical rods of length L sitting at the vertices of an equilateral triangle of sides $d = 1.25L$. Notice the competition between the triplet and pair interactions appearing at $O(d^{-6})$. The pair interactions ultimately dominate and we find the preferred orientations occur for $\theta = 5\pi/6$, in which all rods point inwards.

V. MONOPOLES

Computing interactions that include monopole vertices requires some care. The M_0 polarizabilities are dimensionless, so in order to express the interactions in a proper series in increasing powers of particle size, we must sum up all possible M_0 insertions into each diagram. At first glance this seems daunting, requiring a systematic way to categorize all possible ways to place and permute particle labels on arbitrarily large diagrams while avoiding self-interactions. However, we can save ourselves from intimidating combinatorial gymnastics with a little mathematical rephrasing: For a collection of N particles, M_0 interactions between particles i and j can be thought of as the ijth element of an $N \times N$ matrix $\mathbf{M}$. The sum of all possible M_0 insertions then appears as a *summable* series in powers of $\mathbf{M}$. This approach is particularly manageable for strictly M_0 interactions, so we first focus on the leading-order interaction energy.

A. Leading order

The leading-order interactions consist of *only* M_0 vertices and are given by the infinite series,

$$-\beta\mathcal{U}^{(0)} = \sum_{k\geqslant 1}$$ 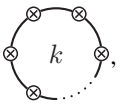 , (71)

where the ⊗ vertex represents an M_0 insertion. This sum can be computed by recasting it in a manner similar to Eq. (50):

$$\begin{aligned}-\beta\mathcal{U}^{(0)} &= \sum_{k\geqslant 0}\frac{1}{2k}\,\mathrm{Tr}(\otimes\!\!-\!\!-)^k = -\frac{1}{2}\,\mathrm{Tr}\log(\mathbf{1}-\otimes\!\!-\!\!-)\\ &= -\frac{1}{2}\log\det(\mathbf{1}-\otimes\!\!-\!\!-)\\ &\equiv -\frac{1}{2}\log\det(\mathbf{1}-\mathbf{M}),\end{aligned} \tag{72}$$

where we have defined the previously mentioned interaction matrix,

$$(\mathbf{M})^{ij} \equiv i\ \cdots\!\otimes\!\!-\!\!-\ j = -M_0^i G^{ij}(1-\delta^{ij}). \tag{73}$$

The indices of $(\mathbf{M})^{ij}$ run over all particle labels, and the factor $(1-\delta^{ij})$ makes explicit the absence of self-interactions. For a collection of N particles, we see the calculation of the leading-order interaction reduces to taking the determinant of the matrix,

$$\mathbf{1}-\mathbf{M} = \begin{pmatrix} 1 & M_0^1 G^{12} & \cdots & M_0^1 G^{1N} \\ M_0^2 G^{21} & 1 & \cdots & M_0^2 G^{2N} \\ \vdots & \vdots & \ddots & \vdots \\ M_0^N G^{N1} & M_0^N G^{N2} & \cdots & 1 \end{pmatrix}, \tag{74}$$

and plugging the result into Eq. (72). For brevity—and with a nod to Ref. [16]—we will express the results using the notation,

$$g_{ij}^2 \equiv M_0^i G^{ij} M_0^j G^{ji} = \frac{\log^2\left(\frac{2\ell_c}{\gamma_e r_{ij}}\right)}{\log\left(\frac{4\ell_c}{\gamma_e s_i^+}\right)\log\left(\frac{4\ell_c}{\gamma_e s_j^+}\right)}, \tag{75}$$

and furthermore introduce the parameter,

$$\Lambda_{ij} \equiv \log\left(\frac{4\ell_c}{\gamma_e\sqrt{s_i^+ s_j^+}}\right), \tag{76}$$

to massage the expression into a form better suited for later expansions:

$$g_{ij} = \frac{\Lambda_{ij} - \log\left(\frac{2r_{ij}}{\sqrt{s_i^+ s_j^+}}\right)}{\Lambda_{ij}(1-\log^2\sqrt{s_i^+/s_j^+})^{1/2}} = 1 - \frac{1}{\Lambda_{ij}}\log\left(\frac{2r_{ij}}{\sqrt{s_i^+ s_j^+}}\right) + \frac{\log^2\sqrt{s_i^+/s_j^+}}{2\Lambda_{ij}^2} + O(\Lambda^{-3}). \tag{77}$$

For two particles we find the interaction energy,

$$\beta\mathcal{U}^{(0)} = \tfrac{1}{2}\log\left(1-g_{12}^2\right). \tag{78}$$

With the help of Eq. (77), we expand this result in powers of $1/\Lambda$ and find the divergences only appear as an irrelevant (infinite) constant:

$$\beta\mathcal{U}^{(0)} = -\tfrac{1}{2}\log\Lambda_{12} + \beta\mathcal{E}_{12} + O(\Lambda^{-1}), \tag{79}$$

where

$$\beta\mathcal{E}_{12} = \frac{1}{2}\log\left[2\log\left(\frac{2r_{12}}{\sqrt{s_1^+ s_2^+}}\right)\right] \tag{80}$$

contains the r-dependent terms. The r dependence, in agreement with [8], shows that at this order the interaction is always attractive.

For three particles, we find

$$\beta\mathcal{U}^{(0)} = \tfrac{1}{2}\log\left[1-\left(g_{12}^2+g_{23}^2+g_{31}^2-2g_{12}g_{23}g_{31}\right)\right]. \tag{81}$$

Contained within this result are both pair and triplet interactions, which we can make explicit by writing

$$\mathcal{U}^{(0)} = \mathcal{U}^{(0)}_{\{1,2\}} + \mathcal{U}^{(0)}_{\{2,3\}} + \mathcal{U}^{(0)}_{\{3,1\}} + \mathcal{U}^{(0)}_{\{1,2,3\}}, \tag{82}$$

where $\mathcal{U}^{(0)}_{\{i,j\}}$ is the pair interaction (79) between particles i and j, and $\mathcal{U}^{(0)}_{\{1,2,3\}}$ is the triplet interaction,

$$\beta\mathcal{U}^{(0)}_{\{1,2,3\}} = \frac{1}{2}\left[\frac{1-\left(g_{12}^2+g_{23}^2+g_{31}^2-2g_{12}g_{23}g_{31}\right)}{\left(1-g_{12}^2\right)\left(1-g_{23}^2\right)\left(1-g_{31}^2\right)}\right]. \tag{83}$$

In the limit of circular particles ($s_i^+ = 2R_i$), we recover the result obtained by a scattering approach in Ref. [16].[6]

To understand the three-particle behavior, we again expand using Eq. (77). After some simplification, the total interaction energy of Eq. (81) becomes

$$\beta\mathcal{U}^{(0)} = -\tfrac{1}{3}\log(\Lambda_{12}\Lambda_{23}\Lambda_{31}) + \beta\mathcal{E}_{\text{tot}} + O(\Lambda^{-1}), \tag{84}$$

with

$$\beta\mathcal{E}_{\text{tot}} = \frac{1}{2}\log\left(\sum_{i,j,k}^{\text{cyc.}\{1,2,3\}}\left[2\log\left(\frac{2r_{ij}}{\sqrt{s_i^+ s_j^+}}\right)\log\left(\frac{2r_{jk}}{\sqrt{s_j^+ s_k^+}}\right) - \log^2\left(\frac{2r_{ij}}{\sqrt{s_i^+ s_j^+}}\right)\right]\right). \tag{85}$$

The triplet (pure three-body) interaction can be found by subtracting off the pairs:

$$\mathcal{E}_{123} = \mathcal{E}_{\text{tot}} - \mathcal{E}_{12} - \mathcal{E}_{23} - \mathcal{E}_{31}. \tag{86}$$

Consider a collection of three identical particles ($s_i^+ = s_+$ for all i) in two different configurations: sitting at the vertices of an equilateral triangle of side lengths d ($r_{12} = r_{23} = r_{31} = d$), and equally spaced on a line ($r_{12} = r_{23} = r_{31}/2 = d$). For the triangle configuration, Eq. (84) reduces to

$$\beta\mathcal{U}^{(0)} = -\log\Lambda + \tfrac{1}{2}\log[3\log^2(2d/s_+)] + O(\Lambda^{-1}), \tag{87}$$

which is overall attractive. To see what role the triplet interaction plays, we can just subtract off the pairs as in Eq. (83). Surprisingly, the triplet and pair interactions have the same d dependence:

$$\beta\mathcal{U}^{(0)}_{\{1,2,3\}} = \frac{1}{2}\log\frac{3\Lambda}{4} - \frac{1}{2}\log\left[2\log\left(\frac{2d}{s_+}\right)\right] + O(\Lambda^{-1}).$$

This pure three-body interaction is in fact repulsive, but not enough so to overcome the attractive pair interactions. For the linear configuration, the total energy is given by

$$\beta\mathcal{U}^{(0)} = \frac{1}{2}\log\left[4\log\left(\frac{2d}{s_+}\right)\log\left(\frac{4d}{s_+}\right) - \log^2\left(\frac{4d}{s_+}\right)\right] - \log\Lambda + O(\Lambda^{-1}), \tag{88}$$

which is also overall attractive. Although it is less obvious than in the triangle configuration, the pure three-body interaction in this case is also repulsive, as can be checked by subtracting off the pairs.

B. Higher orders

To calculate higher orders, we must again include an infinite number of M_0 insertions. This has the effect of replacing each propagator with the sum,

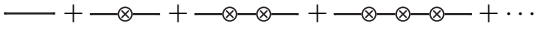

This infinite series, recognized as a type of Dyson equation, is a geometric sum involving powers of $\mathbf{M}$ and is formally convergent in the sense of matrices. Reorganizing the vertex sum gives

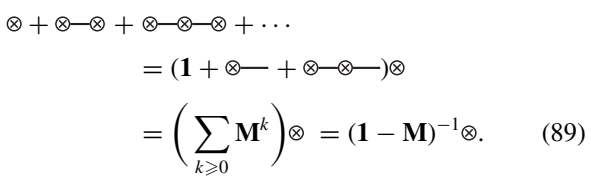

$$= (\mathbf{1} + \mathbf{M} + \mathbf{M}^2)\otimes = \left(\sum_{k\geqslant 0}\mathbf{M}^k\right)\otimes = (\mathbf{1}-\mathbf{M})^{-1}\otimes. \tag{89}$$

This matrix inverse is relatively straightforward to compute, especially for a small number of particles. It follows from the

[6] However, there is a discrepancy with the published version of Ref. [16]; the g^3 term has the opposite sign. We have verified with the authors that this is a typographical error, and our results indeed agree.

Cayley-Hamilton theorem that for N particles, the inverse will contain an overall factor of $1/\det(\mathbf{1}-\mathbf{M})$ and up to $N-1$ powers of $\mathbf{M}$ and their traces.

The vertex sum contains two possibilities: either the vertices begin and end on the same particle worldlines (diagonal entries), or begin and end on different particle worldlines (off-diagonal entries). This motivates grouping the elements of Eq. (89) into the following effective vertices:

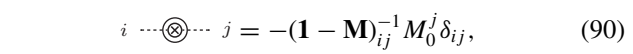

$$= -(\mathbf{1}-\mathbf{M})^{-1}_{ij} M_0^j \delta_{ij}, \tag{90}$$

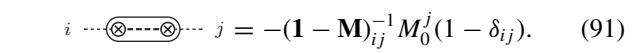

$$= -(\mathbf{1}-\mathbf{M})^{-1}_{ij} M_0^j (1-\delta_{ij}). \tag{91}$$

These effective vertices can be incorporated into interaction diagrams, and the symmetry factors can be determined in the normal way. The interaction energy for (BC 1) is therefore given by

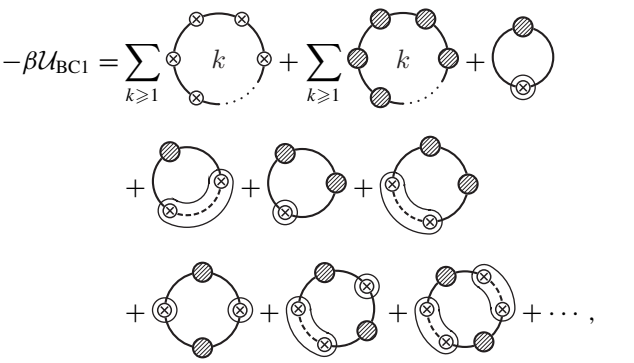

(92)

where the ▨ vertex now contains $M_{n>0}$ terms.

To account for the $M_{n>0}$ terms, first observe that for $n \geqslant m$ the product,

$$(M_0)^n \left(G^{00}_{\alpha\gamma}\right)^m \xrightarrow{\ell_c\to\infty} \delta_{nm}. \tag{93}$$

Since $M_n \propto M_0$, this suggests that for every $M_{n>0}$ vertex in a given diagram, there must be a compensating propagator with no derivatives; otherwise the diagram vanishes. To make this apparent in the diagrams, we represent the M_n and $\bar{M}_n$ vertices, respectively, by

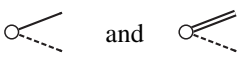

where the dashed line represents (and enforces) a propagator with no derivatives. For example,

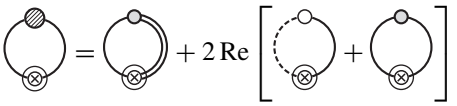

1. Pairs

For two particles, the (2×2) matrix inverse is

$$(\mathbf{1}-\mathbf{M})^{-1} = \frac{\mathbf{1}+\mathbf{M}}{\det(\mathbf{1}-\mathbf{M})},$$

and the effective vertices take particularly simple forms in the limit $\ell_c \to \infty$:

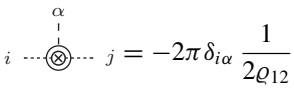

$$= -2\pi\delta_{i\alpha}\frac{1}{2\varrho_{12}}\delta_{\alpha j}, \tag{94}$$

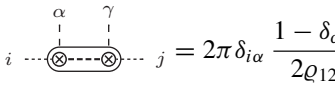

$$= 2\pi\delta_{i\alpha}\frac{1-\delta_{\alpha\gamma}}{2\varrho_{12}}\delta_{\gamma j}, \tag{95}$$

where we have introduced the frequently appearing parameter ϱ_{ij}, which interestingly resembles a screening factor,

$$\varrho_{ij} = \log\left(\frac{2r_{ij}}{\sqrt{s_i^+ s_j^+}}\right) = \frac{1}{2}e^{2\beta\mathcal{E}_{ij}}, \tag{96}$$

where $\mathcal{E}_{ij}$ is the pair energy of (80).

Expanding out the vertices and using the notation,

$$-\beta\mathcal{U}_{\mathrm{BC1}} = -\beta\mathcal{U}^{(0)} + \sum_{\substack{p>0\\ \text{even}}} \frac{u^{(p)}(r)}{r^p},$$

we find the higher-order terms,

$$u^{(2)}_{\mathrm{BC1}} = \frac{1}{16\varrho_{12}}\left[(s_1^+)^2 + 3f_1^2\cos(2\theta_1)\right] + (1\leftrightarrow 2), \tag{97}$$

$$\begin{aligned} u^{(4)}_{\mathrm{BC1}} = u^{(4)}_{\mathrm{BC2}} + \frac{1}{128\varrho_{12}}\big\{&(s_1^+)^4 + 2(s_1^+ s_2^+)^2 \\ &+ 4f_1^2[(s_1^+)^2 + 3(s_2^+)^2]\cos(2\theta_1) + 11f_1^4\cos(4\theta_1) \\ &+ 22f_1^2 f_2^2\cos(2\theta_1+2\theta_2) + (1\leftrightarrow 2)\big\} + \left(u^{(2)}_{\mathrm{BC1}}\right)^2. \end{aligned} \tag{98}$$

At all orders these terms contain contributions with logarithmic prefactors in the form of ϱ_{12}, and they do not vanish in the isotropic limit. These terms exist between two particles, *both* of which are pinned, and they originate from cross-talk between monopoles and higher-order multipoles. They were previously claimed to vanish [13], based on the argument that every diagram involving monopoles and higher-order multipoles vanishes in the limit $\ell_c \to \infty$. However, adding extra monopole insertions to such a diagram does not change its order, hence consistency requires we sum over the complete (infinite) set of insertions, as we have done here. After this resummation, the final result no longer vanishes in the $\ell_c \to \infty$ limit.

The higher-order terms in Eqs. (97) and (98) agree with what has been calculated by Noruzifar *et al.* [8] (up to differing definitions of a and b), except for a prefactor in the last term of Eq. (98). This term is a consequence of the single and double effective vertices limiting to the same value and results from

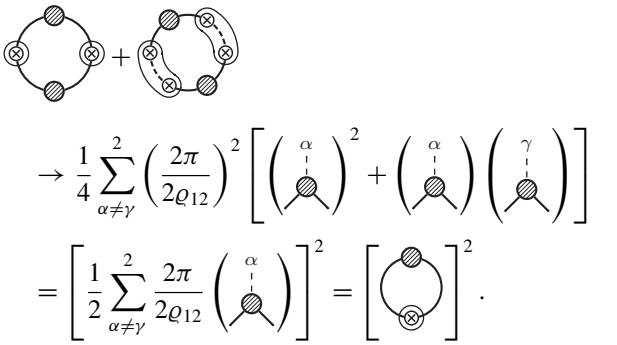

In Ref. [8] it occurs with an extra prefactor of $1/2$, the origin of which is unclear.

We can also compare these results to those obtained using conformal field theory techniques in Ref. [22], for which the authors provide expansions for a couple of special cases. For two identical disks of radius R, and using $x = r/R$, our results reduce to

$$\beta\mathcal{U} = \frac{1}{2}\log(2\log x) - \frac{1}{2x^2\log x} - \frac{1}{x^4}\left(1 + \frac{3}{4\log x} + \frac{1}{4\log^2 x}\right) + \cdots,$$

in agreement with Ref. [22].[7] For two identical aligned rods ($\theta_1 = \theta_2 = 0$) of length L ($s_+ = L/2$ and $f^2 = L^2/4$), our results reduce to

$$\beta\mathcal{U} = \frac{1}{2}\log\left(2\log\frac{4r}{L}\right) - \frac{1}{2(2r/L)^2\log(4r/L)} - \left(\frac{L}{2r}\right)^4\left(\frac{1}{8} + \frac{13}{16\log\left(\frac{4r}{L}\right)} + \frac{1}{4\log^2\left(\frac{4r}{L}\right)}\right) + \cdots$$

If we calculate the total force $F = -\partial_r\mathcal{U}$ and expand in terms of the *tip-to-tip* distance d, we find (with $x = d/(2L)$)

$$2LF = -\frac{1}{2x\log(8x)} + \frac{1+\log(8x)}{4x^2\log^2(8x)} + \cdots,$$

again in agreement with Ref. [22].

2. *Three-body and higher*

For three particles, the (3×3) matrix inverse is given by

$$(\mathbf{1}-\mathbf{M})^{-1} = \frac{\left(1-\frac{1}{2}\operatorname{Tr}\mathbf{M}^2\right)\mathbf{1} + \mathbf{M} + \mathbf{M}^2}{\det(\mathbf{1}-\mathbf{M})}. \tag{99}$$

The $\ell_c \to \infty$ limit for the effective vertices follows after a short calculation, ultimately yielding for the effective single vertex,

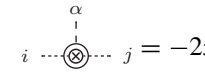

$$= -2\pi\delta_{i\alpha}\frac{2\varrho_{k\ell}}{\sum_{\text{cyc.}}\left(2\varrho_{ab}\varrho_{bc} - \varrho_{ab}^2\right)}\delta_{\alpha j},$$

$$= -2\pi\delta_{i\alpha}\, e^{-2\beta(\mathcal{E}_{k\alpha}+\mathcal{E}_{\alpha\ell}+\mathcal{E}_{123})}\delta_{\alpha j}, \tag{100}$$

where $\alpha,k,\ell \in \{1,2,3\}$ with $\alpha \neq k,\ell$, and $k \neq \ell$ [for example, $(\alpha,k,\ell) = (2,3,1)$]. The second line shows that the effective monopole interaction of particle α effectively "screens" according to its pair (80) and triplet (86) interactions with the other two particles. The effective double vertex becomes

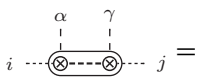

$$= 2\pi\delta_{i\alpha}\frac{\varrho_{\alpha k} + \varrho_{k\gamma} - \varrho_{\alpha\gamma}}{\sum_{\text{cyc.}}\left(2\varrho_{ab}\varrho_{bc} - \varrho_{ab}^2\right)}\delta_{\gamma j},$$

$$= 2\pi\delta_{i\alpha}\frac{1}{2}e^{-2\beta(\mathcal{E}_{123}+\mathcal{E}_{\alpha\gamma})} \times \left[e^{-2\beta\mathcal{E}_{\alpha k}} + e^{-2\beta\mathcal{E}_{k\gamma}} - e^{-2\beta(\mathcal{E}_{\alpha k}+\mathcal{E}_{k\gamma}-\mathcal{E}_{\alpha\gamma})}\right]\delta_{\gamma j}, \tag{101}$$

[7] We have taken the liberty of expanding their result by an additional order for comparison.

in which $\alpha,\gamma,k \in \{1,2,3\}$ with $k \neq \alpha,\gamma$, and $\alpha \neq \gamma$. Note that if there are only two particles, the constraints on α, γ, k, and ℓ reduce both three-body effective vertices to the two-body vertices (94) and (95). However, as long as the system has three pinned particles, the monopole interactions will always be "screened" by the triplet energy, in addition to the pairs.

To demonstrate, we calculate the first subleading correction to the energy of a three-particle configuration:

$$-\beta\mathcal{U}^{(2)} = \frac{1}{8}\sum_{i,j,k}^{\text{cyc.}\{1,2,3\}} e^{-2\beta(\mathcal{E}_{ij}+\mathcal{E}_{jk}+\mathcal{E}_{123})}\frac{1}{r_{ij}^2}\left[(s_i^+)^2 + (s_j^+)^2 + 3f_i^2\cos(2\theta_i) + 3f_j^2\cos(2\theta_j)\right] + \frac{1}{8}\sum_{i,j,k}^{\text{cyc.}\{1,2,3\}}\frac{e^{-2\beta\mathcal{E}_{123}+\mathcal{E}_{jk}}}{r_{ki}r_{ij}}\left[e^{-2\beta\mathcal{E}_{ki}} + e^{-2\beta\mathcal{E}_{ij}} - e^{-2\beta(\mathcal{E}_{ki}+\mathcal{E}_{ij}-\mathcal{E}_{jk})}\right](s_i^+)^2\cos\left(\varphi_{jk}^i\right). \tag{102}$$

The first sum is due to only pairs, whereas the second sum is purely three-body and would vanish in a two-particle system. Observe that the first sum is exponentially suppressed by the leading-order pair energies between one particle and the other two, as well as the triplet energy. This result differs from simply adding the two-particle result (97) pairwise because of this suppression term. We note, however, that the three-particle result is still consistent with the two-particle result—for a two-particle system, $\mathcal{E}_{123}$ and $\mathcal{E}_{jk}$ both vanish in Eq. (102), as does the second sum. Since $e^{2\beta\mathcal{E}_{ij}} = 2\varrho_{ij}$, the result then reduces to Eq. (97). Continuing to even higher orders will follow similarly as straightforward computations of Feynman diagrams, including the proper insertions of the effective monopole vertices.

The "screening" behavior of the monopole interactions by the leading-order pair and multibody energies will persist for more numerous collections of particles. Since, by way of the Cayley-Hamilton theorem, the effective vertices will always carry with them the factor $\det^{-1}(\mathbf{1}-\mathbf{M})$, it follows that all monopole interactions will be exponentially suppressed by the total leading-order multibody monopole energy. As this suppression will always contain multibody energies specific to the total number of particles, these interactions are not just simply sums over partitions (pairwise, tripletwise, and so on) of the collection of particles.

VI. CONCLUSIONS

We have generalized the EFT formalism of fluctuation-induced interactions between particles embedded in a surface to account for possible anisotropies in the particles' shapes. For interactions at large particle separation, the particles can be treated as points with their finite-size effects appearing as a derivative expansion in the effective Hamiltonian. The EFT prescription constrains the possible forms of the individual terms in this expansion through considerations of the particles' symmetries—both the boundary shape and dynamical freedom. By examining and characterizing a hierarchy of relevant system scales, these terms can be ordered in increasing powers of s/r, the ratio of the characteristic particle size and distance

from the particle, allowing systematic control over the desired accuracy of the final results.

We have constructed the general effective Hamiltonian for anisotropic particles in Eq. (8). The coefficients of this expansion have the simple interpretation of polarizabilities: an nth-order multipole background field will induce a multipole response characterized by C_{nm} and χ_{nm} ($m \in \mathbb{N}_0$) in which anisotropies are encoded in the χ and off-diagonal C terms. In the case of ellipses, we could solve for the *complete* set of polarizabilities. This was accomplished by taking advantage of the Hamiltonian's conformal symmetry and mapping the BVP to a simpler problem with a circular boundary. As a consequence of the Riemann mapping theorem, this trick is readily generalizable to particles of any shape. Once a Laurent expansion of the mapping between the particle shape and a disk is determined, up to some desired accuracy, the calculation proceeds just as in Sec. III B.

Once the effective theory has been constructed, the interaction free energy can be computed as a cumulant expansion and identified as a series of connected Feynman diagrams. We discussed the diagrammatics in Sec. IV and calculated the pair interactions to several orders, as well as the leading-order triplet interaction. We found that elliptic particles minimize the free energy by aligning tip to tip and that in three-body configurations the particles will minimize the free energy by aligning their tips to a common center.

Triplet and higher-order interactions become stronger at closer distances, hence they will be especially relevant in dense bulk phases, in which many particles coat a fluid surface. The free energy of such phases can be written as a sum over all pairs, all triplets, and so on. We expect the resulting system to give rise to nontrivial ordered phases; for instance, it is easy to see that a regular triangular lattice would be frustrated, since three close particles minimize their free energy if they all point their tips together, but this is a local conformation that cannot be assumed by every close triplet. While the terms beyond the pair level are only a small correction to the overall free energy, they would shift the location of phase boundaries between such dense phases, but this is beyond the scope of our present work.

We have also provided a detailed examination of the case of fixed particles to elucidate the subtleties of monopole interactions. Field theory has been historically approached by physicists in a manner of "calculate until something goes wrong." The monopole interactions serve as a warning to approach infinite limits with care. In this case, although each M_0-interaction diagram vanishes in the asymptotic limit $\ell_c \to \infty$, the full sum remains finite; the limits do not commute. The resulting resummation shows that the expected powerlike corrections are exponentially suppressed by the leading-order interaction energies.

It is worth emphasizing that in our approach the free energy calculation can proceed even without determining the numerical values of the polarizabilities. The constraints imposed by the particle boundaries provide sufficient information to determine the scaling behavior as well as the angular dependence. For instance, the change in leading-order asymptotics between (BC 2) and (BC 3) from $\sim r^{-4}$ to $\sim r^{-8}$, respectively, is easily seen to be a consequence of the vanishing of the C_{1m} and χ_{1m} polarizabilities. This validates the speculation in Ref. [8] that this is a general feature that holds for arbitrary particle shapes. Furthermore, since the EFT prescription separates out the invariably complicated BVP, the determination of the polarizabilities can be performed in any fashion most convenient for the given problem, even numerically.

ACKNOWLEDGMENTS

We would like to thank Ira Rothstein, Cem Yolcu, and Ehsan Noruzifar for valuable comments and discussions.

APPENDIX A: MONOPOLE ASYMPTOTICS

We first recast the partial differential equation (34) in elliptic coordinates. Under this change of variables, it becomes

$$\frac{1}{f^2(\sinh^2\xi+\sin^2\eta)}\left(\frac{\partial^2\phi}{\partial\xi^2}+\frac{\partial^2\phi}{\partial\eta^2}\right)-\frac{1}{\ell_c^2}\phi=0. \tag{A1}$$

Now, we separate variables by assuming a solution of the form $\phi(\xi,\eta)=R(\xi)\Phi(\eta)$. Plugging this in gives

$$\frac{R''}{R}+\frac{\Phi''}{\Phi}-\frac{f^2}{\ell_c^2}(\sinh^2\xi+\sin^2\eta)=0. \tag{A2}$$

The squares can be removed by using the identities $\sinh^2\xi=(\cosh 2\xi-1)/2$ and $\sin^2\eta=(1-\cos 2\eta)/2$. Letting c be the separation constant, we get two ordinary differential equations (ODEs):

$$R''-\left[\left(c-\frac{f^2}{2\ell_c^2}\right)+\frac{f^2}{2\ell_c^2}\cosh 2\xi\right]R=0,$$

$$\Phi''+\left[\left(c-\frac{f^2}{2\ell_c^2}\right)+\frac{f^2}{2\ell_c^2}\cos 2\eta\right]\Phi=0.$$

Finally, we define $p=c-f^2/2\ell_c^2$ and $q=-f^2/4\ell_c^2$, which puts the ODEs into the form,

$$R''-(p-2q\cosh 2\xi)\,R=0, \tag{A3}$$

$$\Phi''+(p-2q\cos 2\eta)\,\Phi=0. \tag{A4}$$

The angular ODE can be recognized as the Mathieu equation. The periodic boundary condition $\Phi(\eta)=\Phi(\eta+2\pi)$ implies that p depends on a positive integer n. The two families of solutions are given by the (even) cosine-elliptic function $\mathrm{ce}_n(q;\eta)$, where $n\in\mathbb{N}_0$, and the (odd) sine-elliptic function $\mathrm{se}_n(q;\eta)$, where $n\in\mathbb{N}$. The general solution of $\Phi(\eta)$ is then the linear superposition,

$$\Phi_n(\eta)=A_n\,\mathrm{ce}_n(q;\eta)+B_n\,\mathrm{se}_n(q;\eta),\ B_0=0. \tag{A5}$$

With these p_n eigenvalues, the radial ODE becomes the modified Mathieu DE with solutions given by the even and odd evanescent (since $q<0$) radial Mathieu functions of the first kind, $\mathrm{Ie}_n(q;\xi)$ and $\mathrm{Io}_n(-q;\xi)$, and second kind, $\mathrm{Ke}_n(-q;\xi)$ and $\mathrm{Ko}_n(-q;\xi)$. The general solution is again a linear superposition,

$$R_n(\xi)=a_n\,\mathrm{Ie}_n(-q;\xi)+b_n\,\mathrm{Io}_n(-q;\xi)+c_n\,\mathrm{Ke}_n(-q;\xi)+d_n\,\mathrm{Ko}_n(-q;\xi), \tag{A6}$$

where $b_0=d_0=0$. The notation highlights the analogy between the modified Mathieu functions from an elliptic

geometry with the modified Bessel functions of a circular geometry. Indeed, the behavior of the modified Mathieu functions is analogous to the modified Bessel functions: Ke_n and Ko_n decay at infinity, whereas Ie_n and Io_n diverge at infinity. Finally, the complete general solution is given by

$$\phi(\xi,\eta) = \sum_{n=0}^{\infty} R_n(\xi)\Phi_n(\eta). \tag{A7}$$

We could continue and find the explicit solution to our boundary value problem; however, we are only interested in the limiting case of $\ell_c \to \infty$.

Since the capillary length ℓ_c is being used as a regulator, we must consider the solution behavior for $q = -f^2/4\ell_c^2 \to 0$. Although asymptotic series expansions for the Mathieu functions exist in the literature, we can easily get the relevant terms by reconsidering the original differential Equations (A3) and (A4).

The angular solution for $q \to 0$ simply gives $\cos(\sqrt{p}\eta)$ and $\sin(\sqrt{p}\eta)$, but periodicity requires $p = n^2$ for some integer n. For the radial solution, we must be a little more careful since $\cosh 2\xi$ is not bounded above. However, since $\xi \in [0,\infty)$,

$$2q\cosh 2\xi = q(e^{2\xi} + e^{-2\xi}) \sim qe^{2\xi},$$

as $q \to 0$. Recalling that $q < 0$, we introduce an effective elliptic radius $\rho = \sqrt{-q}e^{\xi}$ and rewrite (A3) using $d\rho = \rho\, d\xi$ to give

$$\rho\frac{d}{d\rho}\left(\rho\frac{dR}{d\rho}\right) - (n^2 + \rho^2)R = 0. \tag{A8}$$

This is recognized as the modified Bessel equation, whose solutions $I_n(\rho)$ and $K_n(\rho)$ are the modified Bessel functions of the first and second kind, respectively, again reflecting the analogy with the Mathieu functions.

APPENDIX B: BACKGROUND FIELD RESPONSE

In order to match the monopole polarizabilities, we need a convenient set of background fields as well as the full theory response. Based on the previous section, we should consider the set of background fields,

$$\phi_{\mathrm{bg}}^{(n)} = A^{(n)}\left(\frac{I_n(\rho)}{I_n(\rho_0)}\right)\cos[n(\eta-\varphi)], \tag{B1}$$

where we have included a possible phase φ that may be useful for matching later on, and $\rho_0 = fe^{\xi_0}/2\ell_c = (a+b)/2\ell_c$. The corresponding responses are given by

$$\delta\phi_{\mathrm{full}}^{(n)} = -A^{(n)}\left(\frac{K_n(\rho)}{K_n(\rho_0)}\right)\cos[n(\eta-\varphi)]. \tag{B2}$$

Since $\rho \sim \ell_c^{-1}$, we can simplify matters by taking the asymptotics further, keeping only the singular terms since the remaining terms will vanish in the $\ell_c \to \infty$ limit. To make the expressions more transparent in powers of ℓ_c, we set $\rho \equiv \tilde{\rho}/\ell_c$. The expansions then become

$$\frac{I_n(\tilde{\rho}/\ell_c)}{I_n(\tilde{\rho}_0/\ell_c)} = \left(\frac{\tilde{\rho}}{\tilde{\rho}_0}\right)^n + O\big(\ell_c^{-2}\big), \tag{B3}$$

and

$$\frac{K_n(\tilde{\rho}/\ell_c)}{K_n(\tilde{\rho}_0/\ell_c)} = \begin{cases} \dfrac{\log\left(\frac{\tilde{\rho}}{2\ell_c}\gamma_e\right)}{\log\left(\frac{\tilde{\rho}_0}{2\ell_c}\gamma_e\right)} + O\big(\ell_c^{-2}\big), & n = 0 \\ \left(\dfrac{\tilde{\rho}_0}{\tilde{\rho}}\right)^n + O\big(\ell_c^{-2}\big), & n \geqslant 1, \end{cases} \tag{B4}$$

where $\gamma_e = e^{\gamma_E}$ and γ_E is the Euler-Mascheroni constant. Using the definitions of ρ and $\tilde{\rho}$, the background and response fields finally become

$$\phi_{\mathrm{bg}}^{(n)}(\xi,\eta) = A^{(n)}e^{n(\xi-\xi_0)}\cos[n(\eta-\varphi)], \tag{B5}$$

and

$$\delta\phi_{\mathrm{full}}^{(n)} = \begin{cases} -A^{(n)}\dfrac{\log\left(\frac{fe^{\xi}}{4\ell_c}\gamma_e\right)}{\log\left(\frac{a+b}{4\ell_c}\gamma_e\right)}, & n = 0 \\ -A^{(n)}e^{-n(\xi-\xi_0)}\cos[n(\eta-\varphi)], & n \geqslant 1. \end{cases} \tag{B6}$$

APPENDIX C: INDEPENDENCE OF MATCHING

The conformal transformation of the background field in Sec. III B requires the expansion,

$$\begin{aligned}\left(s_+\frac{w}{R} + s_-\frac{R}{w}\right)^n = &\sum_{\ell<n/2}\binom{n}{\ell}s_+^{n-\ell}s_-^{\ell}\left(\frac{w}{R}\right)^{n-2\ell} \\ &+ \sum_{\ell<n/2}\binom{n}{\ell}s_+^{\ell}s_-^{n-\ell}\left(\frac{R}{w}\right)^{n-2\ell} \\ &+ \mathop{{}^{+}_{\text{even}}}\binom{n}{n/2}(s_+s_-)^{n/2},\end{aligned} \tag{C1}$$

where the last term only appears when n is even (hence the "$\mathop{{}^{+}_{\text{even}}}$" notation). As seen in Eqs. (B5) and (B6), a nonzero constant background generates a monopole response. In particular, the response to the full constant term in w space is similar to (B6) and given by

$$\delta\phi_C = -\frac{A^{(n)}(s_+s_-)^{n/2}}{2^n}\binom{n}{n/2}\frac{\log\left(\frac{|w|\gamma_e}{2\ell_c}\right)}{\log\left(\frac{R\gamma_e}{2\ell_c}\right)}(e^{-in\varphi} + e^{in\varphi}). \tag{C2}$$

Since there is no singular behavior in mapping back to the ellipse via $w \to w(z)$, we can safely take the limit $\ell_c \to \infty$, giving

$$\delta\phi_C = -\frac{A^{(n)}}{2^n}\binom{n}{n/2}(s_+s_-)^{n/2}(e^{-in\varphi} + e^{in\varphi}). \tag{C3}$$

Now let's consider the effect of the background field in the monopole EFT in (38). From $\phi_{\mathrm{bg}}^{(n\geqslant 1)}(0) = 0$ and $\partial^m\phi_{\mathrm{bg}}^{(n\geqslant 1)}(0) = A^{(n)}n!\delta_{mn}e^{-in\varphi}$, we see the only nonvanishing term is

$$\begin{aligned}\delta\phi^M &= \sum_{\substack{n>0\\ \text{even}}}\frac{M_n}{2\pi}\log\left(\frac{|z|\gamma_e}{2\ell_c}\right)\partial^n\phi_{\mathrm{bg}}(0) + \text{c.c.} \\ &= -\sum_{\substack{k>0\\ \text{even}}}\frac{\log\left(\frac{|z|\gamma_e}{2\ell_c}\right)}{\log\left(\frac{(a+b)\gamma_e}{4\ell_c}\right)}\frac{f^kA^{(n)}n!\delta_{kn}e^{-in\varphi}}{2^k\left[\left(\frac{k}{2}\right)!\right]^2} + \text{c.c.},\end{aligned}$$

$$\xrightarrow{\ell_c\to\infty} -\frac{f^nA^{(n)}n!}{2^n\left[\left(\frac{n}{2}\right)!\right]^2}(e^{-in\varphi} + e^{in\varphi}) \quad (n \text{ even}). \tag{C4}$$

Recalling that $f^n = (s_+ s_-)^{n/2}$ and $\binom{n}{n/2} = n!/[(\frac{n}{2})!]^2$, we find (C4) is precisely equal to (C3). Therefore, we find that the higher-order polarizabilities can be matched independently of the monopole terms without contamination by simply ignoring the constant term in the binomial expansion of Eq. (C1).

[1] H. B. G. Casimir, Proc. K. Ned. Akad. Wet. **51**, 793 (1948).
[2] K. A. Milton, *The Casimir Effect: Physical Manifestations of Zero-point Energy* (World Scientific, River Edge, 2001).
[3] M. Kardar and R. Golestanian, Rev. Mod. Phys. **71**, 1233 (1999).
[4] A. Gambassi, A. Maciołek, C. Hertlein, U. Nellen, L. Helden, C. Bechinger, and S. Dietrich, Phys. Rev. E **80**, 061143 (2009).
[5] H. Lehle, M. Oettel, and S. Dietrich, Europhys. Lett. **75**, 174 (2006).
[6] H. Lehle and M. Oettel, Phys. Rev. E **75**, 011602 (2007).
[7] H. Lehle, E. Noruzifar, and M. Oettel, Eur. Phys. J. E **26**, 151 (2008).
[8] E. Noruzifar and M. Oettel, Phys. Rev. E **79**, 051401 (2009).
[9] H. Li and M. Kardar, Phys. Rev. Lett. **67**, 3275 (1991).
[10] R. Golestanian, M. Goulian, and M. Kardar, Europhys. Lett. **33**, 241 (1996).
[11] R. Golestanian, M. Goulian, and M. Kardar, Phys. Rev. E **54**, 6725 (1996).
[12] C. Yolcu, I. Z. Rothstein, and M. Deserno, Europhys. Lett. **96**, 20003 (2011).
[13] C. Yolcu, I. Z. Rothstein, and M. Deserno, Phys. Rev. E **85**, 011140 (2012).
[14] C. Yolcu and M. Deserno, Phys. Rev. E **86**, 031906 (2012).
[15] E. Noruzifar, J. Wagner, and R. Zandi, Phys. Rev. E **87**, 020301 (2013).
[16] E. Noruzifar, J. Wagner, and R. Zandi, Phys. Rev. E **88**, 042314 (2013).
[17] I. Z. Rothstein, Nucl. Phys. B **862**, 576 (2012).
[18] T. Emig, N. Graham, R. L. Jaffe, and M. Kardar, Phys. Rev. Lett. **99**, 170403 (2007).
[19] T. Emig, N. Graham, R. L. Jaffe, and M. Kardar, Phys. Rev. D **77**, 025005 (2008).
[20] B. B. Machta, S. L. Veatch, and J. P. Sethna, Phys. Rev. Lett. **109**, 138101 (2012).
[21] O. A. Vasilyev, E. Eisenriegler, and S. Dietrich, Phys. Rev. E **88**, 012137 (2013).
[22] G. Bimonte, T. Emig, and M. Kardar, Europhys. Lett. **104**, 21001 (2013).
[23] S. A. Safran, *Statistical Thermodynamics of Surfaces, Interfaces, and Membranes* (Perseus, Cambridge, 1994).
[24] I. Z. Rothstein, arXiv:hep-ph/0308266v2.
[25] T. Emig, N. Graham, R. L. Jaffe, and M. Kardar, Phys. Rev. A **79**, 054901 (2009).